

Low Frequency Noise in the Single Electron Transistor: Instrumentation and Experiments

Björn Starmark

Licentiate thesis/Licentiatuppsats

Institutionen för Mikroelektronik och Nanovetenskap
Chalmers Tekniska Högskola och Göteborgs Universitet
1998-10-08

Low Frequency Noise in the Single Electron Transistor: Instrumentation and Experiments

Björn Starmark

8th October 1998

Abstract

This is a study of low frequency noise of the Single Electron Transistor (SET). SETs are the most sensitive electrometers existing today, and have sub-electron sensitivity ($2 \cdot 10^{-5} e/\sqrt{Hz}$). They are predicted to have quantum limited sensitivity, *i.e.* the sensitivity is determined by Heisenbergs uncertainty relation. However, a problem with SETs is the low signal bandwidth which lowers the sensitivity at frequencies above 1-5 kHz. Also, at these low frequencies another noise process, so called $1/f$ noise, masks the potential sensitivity. As a consequence, no one has so far proved the quantum limit hypothesis.

In order to gain knowledge of the origin of the $1/f$ noise, a study of low frequency noise of the SET was performed. and *Al*-based *Nb/Al*-based SET transistors were fabricated in the Swedish Nanometer Laboratory using nanolithographic techniques. To improve noise readout, a low noise, current sensitive preamplifier was designed and built, which was then used in the experiments. It has a major advantage over the commonly used voltage sensitive preamplifier in that the bandwidth is increased. An understanding of the preamplifier characteristics was necessary for noise data interpretation. Relevant preamplifier characteristics are discussed.

Noise was then measured in the frequency band 1 Hz -5 kHz. In this range the transistors showed a $1/f^{1.6}$ dependent spectrum, which is in accordance with other investigations. By investigating many bias points (> 100), it was found that the output noise clearly followed the small-signal gain of the transistor. This implies that the major noise contribution comes from noise sources acting at the input of the transistor. For high bias voltages, a small noise contribution was found that could not be explained as being caused by input acting noise sources. A simple phenomenological noise model explained the extra noise contribution as resistance fluctuations of the transistor tunnel junctions. These fluctuations were estimated for both transistors.

Contents

1	Introduction	3
1.1	The Coulomb Blockade	3
1.2	The Single Electron Transistor and its Characteristics	4
1.2.1	Island Charging Energy	4
1.2.2	Tunnel Resistance Dependence	5
1.2.3	Frequency Performance	6
1.2.4	The Superconducting SET	6
1.2.5	Small Signal Characteristics	7
1.3	SET Noise	8
1.4	Filtering	8
1.5	Summary	8
1.6	Author Contribution	8
2	SET Noise Properties	10
2.1	High Frequency Noise	10
2.2	Quantum and Thermal Noise	10
2.3	Low Frequency Noise	11
2.3.1	LF Noise Observations	11
2.3.2	Input and Output Noise Sources Contributions	13
2.3.3	Phenomenological Low Frequency Noise Model	14
3	Experimental Techniques	16
3.1	Sample Fabrication	16
3.2	Cryogenics	17
3.3	Measurement Setup	17
3.4	Crosstalk	17
3.5	Current Preamplifier Review	18
3.5.1	Introduction	18
3.5.2	DC properties	19
3.5.3	AC properties	21
3.5.4	Noise Properties	24
3.5.5	Stability	25
3.5.6	Differential Current Preamplifier	26
3.5.7	Voltage Bias Precautions	27

4	Results	28
4.1	Preamplifier Performance	28
4.2	SET Results	29
4.2.1	High Ohmic SET	29
4.2.2	Low Ohmic SET - Normal State	30
4.2.3	Low Ohmic SET - Superconducting State	31
4.2.4	Superconducting and Normal SET Noise Spectra	31
4.2.5	Low Frequency Noise	34
4.3	Niobium SET Noise Characteristics	36
4.4	Discussion and Future work	36
5	Conclusions	39
6	Acknowledgements	40
A	List of Symbols	45
B	Appended Paper 1	49
C	Appended Paper 2	55
D	Appended Paper 3	67

Chapter 1

Introduction

1.1 The Coulomb Blockade

The discreteness of electric charge [1,2], has consequences which are not obvious at first sight. Imagine a capacitor being charged by a single electron. An energy has to be overcome to allow this process. The energy is simply the charging energy of the capacitor, given by $E = \frac{e^2}{2C}$, where e is the charge of the electron and C is the capacitance of the capacitor. For ordinary capacitors used in electronics, C is usually somewhere between 1 pF and 1 F, which corresponds to energies of $90 \cdot 10^{-9}$ eV or less. These energies are so small that the thermal fluctuations of electrons in equilibrium at room temperature is much greater, $k_B T = 26$ meV. However, if the capacitor and the temperature of the electrons can be made small enough, the electrons are repelled from the capacitor. This charging effect is a purely classic concept based on Maxwell's equations.

If the dielectric material between the plates of the capacitor is made very thin (~ 10 Å), another phenomenon sets in; tunneling. The electrons can jump through the ~ 10 Å isolating dielectric and end up on the opposite electrode. From an electronics point of view, this is a non-ideal capacitor, since the charge stored on it can leak away. This type of capacitor is usually called a *tunnel junction*. The imperfect isolator has a *tunnel resistance* that limits the current through the junction. Now by connecting two such tunnel junction in series, the two interconnected middle electrodes forms an isolated island, as shown in Fig.(1.1). If a small bias voltage is applied to the electrodes, the current through the structure will be blocked by the energy barrier due to the charging energy of the island. This is called the Coulomb Blockade of single electron tunneling. For larger bias voltages, the barrier is overcome, tunneling is allowed and a current will flow.

If an external electric field is applied on the island, it becomes polarized, *i. e.*, charge is induced. As a consequence, the Coulomb Blockade can be detuned and the potential barrier is removed, allowing free transport across the junctions. This tuning property forms the basis of the Single Electron Transistor (SET) [3]. The external field is usually applied by a gate near the island. It is galvanically (but not electrostatically) isolated from the island, giving the device a very high input impedance. SETs have been fabricated since 1987 [4], and show many interesting properties.

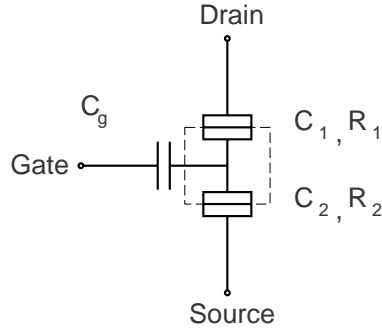


Figure 1.1: Two tunnel junctions in series creates an isolated island. External fields landing there induce charge. The field can detune the Coulomb Blockade, allowing free tunneling across the two capacitors.

By connecting tunnel junctions in different ways, other circuit types are formed. Among these are the Single Electron Turnstile [5], the 1D Array [6] and the Single Electron Pump [7,8]. Common to all these circuits is that they allow control of the electric current on the single electron level. This field of physics is commonly called Single Electronics [9].

1.2 The Single Electron Transistor and its Characteristics

A transistor based on the Coulomb Blockade was first proposed by Likharev [3]. The theory originally developed goes under the name 'the Orthodox theory' of single electron tunneling [10]. It predicted that the SET should have an extreme sensitivity to external electric fields. Used as a charge sensor, sub-electron sensitivity was predicted. In 1987, Fulton and Dolan successfully demonstrated the first (lithographically defined) working SET [4]. This started a great activity in the field of single electronics. Soon other groups mastered the technology and many new circuits have since then been studied. The basic SET properties are by now well known. The DC properties are reviewed below, while noise characteristics will be discussed in Chapter 2. It is assumed that the reader understands the basic principles on which the SET relies on. Readers without prior knowledge are referred to Ref. [10].

1.2.1 Island Charging Energy

The energy scale of the system is set by the charging energy of the metallic island. The island capacitance is usually written C_Σ and is the sum the junction capacitances, C_1, C_2 , the gate capacitance, C_g , and the island self capacitance, C_0 , *i.e.*

$$C_\Sigma = C_1 + C_2 + C_g + C_0 \quad (1.1)$$

Typical values for aluminum SETs are $C_1, C_2 \approx 0.1 - 10$ fF, $C_g \approx 1 - 1000$ aF and $C_0 \approx 3 - 30$ aF. The charging energy, E_C is given by

$$E_C = \frac{e^2}{2C_\Sigma} \quad (1.2)$$

With today's lithographic techniques, energies on the order of ~ 1 K are easily achievable. The temperature must then be below 100 mK for proper operation. Dilution refrigerators (cryostats) are required to reach these temperatures. The low operating temperature is the most important drawback of the metallic SET. At NEC, optimized lithography techniques have pushed this limit to above 77 K [11]. However, the reproducibility is then lower.

1.2.2 Tunnel Resistance Dependence

For bias voltages well above the offset voltage, the current through the SET is limited by the combined resistance of the two tunnel junctions. The resistance is sometimes called the asymptotic resistance,

$$R_N = R_1 + R_2 \quad (1.3)$$

where R_i is the tunneling resistance of junction 1 or 2. In order to operate properly, the island must be isolated from the electromagnetic environment to prevent charge from leaking out. To get a pronounced blockade, R_N must be greater than the resistance quantum, R_Q [10], defined as

$$R_Q = \frac{h}{4e^2} \approx 6.45\text{k}\Omega \quad (1.4)$$

If the resistance is lower than this, the charge on the island is not well defined and the sensitivity to external fields disappears. This is due to *cotunneling* [12], which will smear the blockade for low enough R_N . An example of this is shown in Fig.(1.2). The SET with higher R_N , $R_N = 415$ k Ω , has a more well defined blockade than the low ohmic SET ($R_N = 45$ k Ω). Making R_N higher than 500 k Ω doesn't change the blockade much. To achieve large voltage modulation, ΔV , a high resistance is needed. On the other hand, it has been shown that the blockade can survive for a resistance below R_Q [13,14] and the SET can still be modulated. Since R_N is low, the *current* modulation, ΔI , is actually higher for moderately values of R_N than for high values. This is because the tunneling rate is set by $\frac{1}{R_N C_\Sigma}$ for high R_N . For constant C_Σ , there should be an optimum current modulation for some finite R_N above R_Q . It is possible to estimate this optimum transistor resistance $R_{N,opt}$. In low ohmic systems, the current modulation is, according to D. Golubev, [15], reduced by a factor $e^{-2\alpha_t}$, where $\alpha_t \equiv \frac{4R_Q}{R_N}$. This is due to the smeared blockade. The total current modulation then becomes

$$\Delta I = \frac{e}{R_N C_\Sigma} e^{-2\alpha_t} \quad (1.5)$$

The maximum for ΔI is then found for

$$R_{N,opt} = \sqrt{2}4R_Q \approx 37\text{k}\Omega \quad (1.6)$$

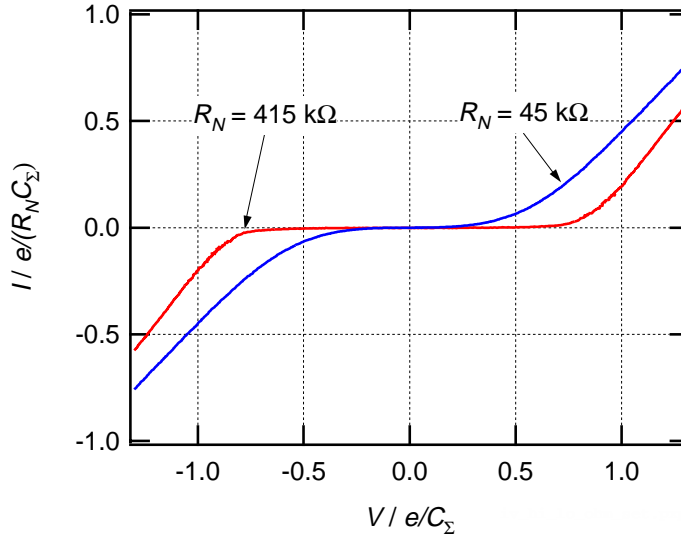


Figure 1.2: Normalized current-voltage (IV) characteristics for two SETs with different asymptotic resistance. The low ohmic SET shows considerable smear viz. the high ohmic SET.

and the corresponding current modulation is

$$\Delta I = \frac{e}{4\sqrt{2}R_Q C_\Sigma} e^{-1/\sqrt{2}} \approx 3 \cdot 10^{-6} \frac{e}{C_\Sigma} \quad (1.7)$$

One has to remember that this is an approximation and the real value is probably dependent on other parameters, such as the technology used.

1.2.3 Frequency Performance

The high resistance leads to a bandwidth problem. Since operation is limited to within a cryostat, long measurement leads from the SET to the room temperature electronics are needed. These leads have parasitic capacitances which together with the SET resistance form a low pass filter. Typical cutoff frequencies are on the order of 300 Hz. Recently, the bandwidth of the SET was dramatically increased to over 100 MHz [16]. This was accomplished by using a radio frequency read-out method. A SET operating in this mode is referred to as the RF SET. The method provided large bandwidth and low noise. However, the ultimate noise performance level (see below) was not reached. The drawbacks of this method is that it requires expensive high frequency equipment and that black-body radiation filtering (see Sec(1.4) below) becomes difficult.

1.2.4 The Superconducting SET

Aluminum SETs operated below $T = 1.2 - 1.5$ K become superconducting. The superconductivity introduces an energy gap, Δ , around the Fermi energy where

no electronic states are available. If the Josephson Energy $E_J = \frac{\Delta}{2} \frac{R_Q}{R_N}$ is small, an extra energy on top of the Coulomb Gap is needed to pass a current through the device. The superconductivity has at least two positive effects [17–19].

1. The operating temperature is increased:

$$k_B T_{op} < 2\Delta + E_C \quad (1.8)$$

2. ΔI is increased. Naively, one would get

$$\Delta I \approx \frac{2\Delta + E_C}{R_N} \quad (1.9)$$

This is not a very exact estimate however, and the real increase may depend on details in the density of states of the electron states [19]. Furthermore, effects of the output impedance (see Sec.(1.2.5)) may also limit the increase.

One possible consequence is that E_C does not need to be very large to see appreciable modulation, as long as the gap is large. The modulation dependence on low charging energy and low asymptotic resistance has not yet been examined in the superconducting state. From a device point of view, this is an interesting region due to the potential for higher current modulation. SETs based on materials with large superconducting gaps, such as niobium, may also profit from this.

1.2.5 Small Signal Characteristics

From a device point of view, the two most important small signal parameters are the gain and the output impedance, also known as the dynamic resistance. The values of these parameters are needed to predict the performance of a SET connected to a preamplifier. When used as a voltage biased electrometer, the charge gain is written as η and is defined from the modulation characteristics as

$$\eta \equiv \left(\frac{\partial I}{\partial Q_g} \right)_V \quad (1.10)$$

If the SET is operated as a voltage sensor, the gain is the transconductance, g_m , which is defined in the usual way as

$$g_m \equiv \left(\frac{\partial I}{\partial V_g} \right)_V \quad (1.11)$$

The charge gain and the transconductance are related by the gate capacitance C_g :

$$g_m = C_g \eta \quad (1.12)$$

The output impedance is written r_o and is defined from the IV characteristics as

$$r_o \equiv \left(\frac{\partial I}{\partial V} \right)_{Q_g} \quad (1.13)$$

For the noise analysis, the junction current dependence on resistance is defined by

$$\kappa_i \equiv \left(\frac{\partial I}{\partial R_i} \right)_{Q_g} \quad (1.14)$$

where i denotes junction number.

1.3 SET Noise

The SET is predicted to have an extremely high charge sensitivity [20]. The sensitivity is limited by the shot noise of the bias current. For very low temperatures and small bias voltages, the quantum fluctuations of the charge should set the ultimate limit. The SET is in other words a quantum limited charge sensor. This limit has not been reached in any SET experiments so far,. Either the bandwidth is too low, or the preamplifier adds to much noise (as in the RF SET).

At low frequencies, the SET shows a noise contribution that increases as the frequency decreases. This is called $1/f$ noise due to its frequency scaling. Due to the small bandwidth and this extra noise contribution, the predicted charge sensitivity has not yet been achieved. Therefore, much attention is now given to these problems. Low frequency noise is studied by many groups [17, 18, 21–26]. The noise is believed to be caused by a small two level system, either in close vicinity to the island, or inside a barrier. Each such atomic (or molecular) system randomly jumps between two charge states. Due to its high sensitivity, the SET picks up the noise caused by the switching. The location of these fluctuators is still an open question.

1.4 Filtering

When the SET was operated in a cryostat, it was found that black body radiation from 'warm' parts (≥ 1.2 K) could trigger parasitic tunneling events by photon assisted tunneling. To overcome this problem, filters that absorb this radiation have been designed. Several types of filters have been investigated [27, 28]. Among these is the so called Thermocoax filter, [27], which is a coaxial cable with a special dielectric that has a very high absorption of microwaves (Normally, Thermocoax is used as a heating wire in vacuum environments). All these filters have a drawback in that they add to the lead capacitance, further lowering the bandwidth.

1.5 Summary

The conclusions from the section above are: one, the SET has a potential as a quantum limited charge sensor. Two, due to limitations in lithography, metallic SETs are limited to low temperature operation. Often, the SET has then to be cooled in a cryostat, which limits the bandwidth due to long measurement leads. Three, at low frequency, the noise is dominated by a $1/f$ noise contribution which masks the potential sensitivity.

1.6 Author Contribution

The work presented in this thesis attacks two problems. The first part, presented in appended paper 1, aimed to increase the bandwidth by using a current sensitive preamplifier (hereafter referred to as the preamp). The preamp was designed, partly built and tested by the author. Its characteristics are discussed

in detail in Sec.(3.5), and can be skipped by the casual reader. The conclusions from this discussion are found in Eqs.(3.10) and (3.12). These equations describes the transfer function and the added noise of the preamp, which are needed in discussing the results.

The goal of the second part, presented in appended papers 2 and 3, was to investigate the low frequency noise of the SET. To this end, software drivers for the noise measurement equipment used was developed by the author. Furthermore, an experimental methodology was formed during the first experiments. This included guidelines for choosing the bias points, gain estimation and bandwidth correction methods. This work was done by the author.

Using a phenomenological model derived by A.N. Korotkov [29], a separation into charge and resistance noise was possible. Both *Al* based and *Nb* based devices were investigated. The aluminum SETs were fabricated and noise characterized by the author. T. Henning fabricated and characterized the niobium transistors using the preamp, software and some of the methods developed by the author. Mainly the results of the *Al* SETs are discussed in this thesis. The model is discussed in Sec.(2.3.2) and the results are presented in Sec.(4.2).

Chapter 2

SET Noise Properties

2.1 High Frequency Noise

The high frequency noise properties of the SET have been calculated by Korotkov *et al.* [20]. For frequencies well below the inverse mean tunneling time ($t = R_{\Sigma}C_{\Sigma}$) the output current noise spectrum, $S_I(\omega)$, shows shot noise [30]. This is caused by electrons tunneling across the junctions. For bias voltages below the threshold *i.e.* $V < V_T \equiv \frac{e^2}{2C_{\Sigma}}$ half shot noise is obtained, $S_I(\omega) = eI$. This is due to correlated tunneling. For $V > V_T$, the tunneling events are the uncorrelated and the SET should show full shot noise, $S_I(\omega) = 2eI$. These results have been experimentally confirmed for a double-junction structure (*i.e.* a SET without gate) using an STM tip as one of the junctions [31]. The shot noise of a SET and the corresponding charge sensitivity is yet to be observed. The current levels in metal-insulator-metal SETs are in the 1 pA - 10 nA range, which gives shot noise levels of 0.6 - 60 fA/ $\sqrt{\text{Hz}}$. The corresponding charge sensitivity should be in the range 2-10 $\cdot 10^{-6}e/\sqrt{\text{Hz}}$.

2.2 Quantum and Thermal Noise

According to Korotkov *et al.* [20], the minimum charge noise achievable is

$$q_{n,min} = 5.4\sqrt{k_B T R_{min} C_{min}} \approx 2.7\sqrt{k_B T R_{min} C_{\Sigma}} \quad (2.1)$$

where the last equality assumes a symmetric transistor. As temperature decreases, the charge noise decreases. For some low temperature, the thermal fluctuations becomes lower than the quantum fluctuations. Quantum fluctuations in the charging energy of the SET should set the ultimate low noise limit of the SET [23]. The quantum energy fluctuations are given by Heisenberg's uncertainty relation, $\Delta E \Delta t \geq \hbar$. Δt is the life time of the charge of the island and is on the order of $\Delta t \sim R_{min} C_{\Sigma}$. This gives

$$\Delta E \sim \frac{\hbar}{R_{min} C_{\Sigma}} \quad (2.2)$$

By substituting $k_B T$ with eq.(2.2), the quantum limited charge noise is obtained:

$$q_{n,min} = 2.7\sqrt{\hbar C_{\Sigma}} \quad (2.3)$$

If an energy sensitivity, E_N , is defined as $E_N = \frac{q_n^2}{2C_\Sigma}$ [20], the minimum energy sensitivity becomes $E_N = 3.6\hbar$. Thus, the SET is potentially a quantum limited charge sensor since its minimum energy sensitivity is of order \hbar . In Ref. [23], the SET was predicted to have $E_N = 1.5\hbar$, which corresponded to $q_{n,min} \sim 2.2 \cdot 10^{-6} e/\sqrt{\text{Hz}}$.

One DC effect of the quantum noise is found in Fig. (1.2). The low ohmic SET shows a considerable smear around the blockade. This smear could be caused by thermal fluctuations of the charge state. However, both SETs were measured at temperatures well below the charging energy. From Sec.(1.2.2), the smear is caused by cotunneling, which gives an uncertainty in the charge state. This is then interpreted as quantum fluctuations of this state.

2.3 Low Frequency Noise

For low frequencies (LF), the shot and/or quantum fluctuations are masked by other noise mechanisms. The current noise spectrum shows a $1/f^\alpha$ dependence with $1 \leq \alpha \leq 2$. This is called $1/f$ noise and is a general phenomenon present in all types of electronic components (passive and active) (see *e.g.* [32, p. 432]). The presence of the $1/f$ noise severely limits the LF sensitivity of the SET. Many studies on metal-insulator-metal SETs have been performed in order to determine the origin of the LF noise [17, 18, 21–26, 33–38]. Important results from these studies are reviewed below.

2.3.1 LF Noise Observations

Generally, low frequency noise data is collected within the frequency band $10^{-3} \text{ Hz} \leq f \leq 10^3 \text{ Hz}$. The lower limit is set by the measurement time. A frequency of 10^{-3} Hz corresponds to approx. 17 minutes per spectrum. Usually, 100 spectra are required to get good statistics (10 % error), corresponding to 28 hours measurement *per bias point*. For many SETs, it is impossible to keep the gate bias stable for such a long period of time. Sudden charge jumps offset the gate charge anywhere within a fraction of an electron. The upper frequency limit is set by the combination of the SET dynamic output resistance and the capacitive load of the measurement leads (see Sec.(3.2)).

Different types of spectra are shown in Fig.(2.1). The measured spectra have a region where the noise shows a $1/f^\alpha$ dependence, with $1 \leq \alpha \leq 2$. In some experiments, the spectra show pure $1/f$ behavior for the lowest frequencies. In other experiments, a Debye-Lorentzian spectrum is observed. The spectrum saturates at a constant value for the lowest frequencies, and rolls off as $1/f^2$ for higher frequencies. A characteristic switching between two (or more) levels is usually observed in connection with the Debye-Lorentzian spectrum. This is also called telegraph noise, popcorn noise or burst noise and is also observed in semiconductor devices (see *e.g.* [39, p. 142]). Theoretically, the spectrum and the switching can be explained as caused by a system which randomly jumps between two discrete states [40]. Such a system is usually called a two level fluctuator (TLF). In the SET, it is believed that the TLFs consist of charge traps, where an electron randomly switches between two states [18, 23, 24]. If two or more TLFs are active, the switching occurs between many discrete states. Also, the spectrum is then a superposition of many Debye-Lorentzian spectra.

In the limit of an infinite number of TLFs, it has been shown that the spectrum will become a $1/f$ spectrum (see [39, Chapter 8]).

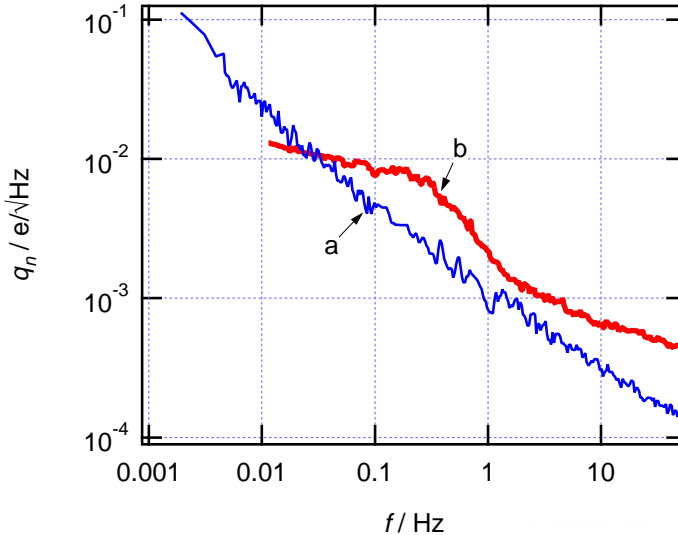


Figure 2.1: Example of different types of low frequency noise spectra observed in SETs. Curve (a) has a $1/f$ dependence, while curve (b) is a superposition of a Debye-Lorentzian spectrum and a $1/f$ background. Data taken from Ref. [23] (a) and Ref. [34] (b).

In order to lower the LF noise, the location of the traps has to be found. There are three main candidates for the location [24]:

- 1.) the tunnel junction dielectric
- 2.) the substrate
- 3.) the metal oxide covering the island

The first candidate is discussed in Ref. [41]. There, large area Josephson junctions were studied, and the TLFs were found to be located in the tunnel junction dielectric. The junctions were low-ohmic, had large area and based on a Nb/Pb alloy, commonly used in SQUIDs. In Ref. [18], Song et al. proposed that the situation is the same for SETs. They based their proposal on the fact that the TLF must be located very close to the island in order to modulate the SET with a charge corresponding to one electron. However, Zorin *et al.* [24] pointed out that the electric field in a SET junction oscillates with a period set by the mean tunneling time which is less than 1 ns. This is in contrast to large area junctions where the field is constant. It is difficult to imagine a TLF producing a Debye-Lorentzian spectrum while being shaken by a GHz electric field. Furthermore, they [24] carried out a correlation experiment involving two closely situated SETs to see if the noise source was common to both SETs. It was found that a considerable part of the noise was indeed common. Also, they calculated that TLFs close to the island can modulate the SET considerably, even though they aren't located in the junction dielectric. Thus, the substrate and the metal oxide cover are possible locations for the TLFs. Further evidence

for this was provided by Zimmerman *et al.* [42]. They were able to show that the TLFs in their SET were *not* located inside the barrier. However, it must be noted that in their sample, the charge noise was unusually high with a total charge switching on the order of an electron. Such a high level of noise could possibly mask other noise sources including junction dielectric TLFs.

A recent experiment hints that the TLFs are located in the substrate/island interface [37]. By placing the island partly on top of the bottom electrode, the contact area of the island to the substrate was minimized. The LF noise was dramatically reduced, and one of the samples set a new sensitivity record of $q_n \approx 2.5 \cdot 10^{-5} e / \sqrt{\text{Hz}}$ at 10 Hz. Another sample showed anomalous behavior. The output current noise spectrum $S_I(\omega)$ was independent on gain but dependent on bias current. Furthermore, $S_I(\omega)$ was constant in the 0.1-100 Hz range, *i.e.* white noise. The noise level was too high to be shot noise. The authors concluded that conductance fluctuations were the sources of the noise.

Two conclusions can be drawn from these experiments:

1.) the two first experiments showed that the TLFs are probably not in the junction dielectric. This leaves the substrate and the metal oxide as possible locations.

2.) the third experiment showed that the LF noise can be substantially reduced by minimizing the substrate/island contact area. This is a very important result which may lead to further noise reduction. Furthermore, conductance fluctuations can occur in this new layout.

It should be mentioned that different substrate materials does not seem to lower the noise more than a factor 2 [25]. The most widely used substrate is *Si* or *Si* with a thick *SiO₂* layer. It is well known that the *Si/SiO₂* interface can contain large amounts of defects [43]. These defects acts as TLFs. In the semiconductor industry, passivation of the *Si* surface with hydrofluoric acid effectively reduces the trap density. To investigate the strength of these traps, experiments at Chalmers are under way where SETs are fabricated on passivated *Si* substrates.

2.3.2 Input and Output Noise Sources Contributions

In the section above, it was concluded that the LF noise contains one large charge noise contribution and possibly, a smaller conductance noise contribution. The problem is how to experimentally measure and separate these contributions. One possible approach is outlined in appended paper 2, and is based on input and output noise sources. The separation into input and output noise sources has a strong physical motivation. At low frequencies, TLFs in the substrate would only induce charge or input noise $S_{in}(f)$. On the other hand, TLFs in the junction dielectric would induce charge noise as well as conductance noise at the output of the device, $S_{out}(f)$. At high frequencies, the shot noise is clearly generated at the output of the device; then $S_{out}(f) = aeI$ (and if $S_{in}(f) = S_{Q_g}(f)$, $S_{in}(f)$ should decrease as $1/f^\alpha$, which is true for all experiments conducted so far).

The separation is very simple. Assume a voltage biased SET and that the output current spectrum $S_I(f)$ is measured. Noise sources acting at the gate of the SET with spectrum $S_{in}(f)$ will be amplified by the gain η . Noise sources acting at output of the SET with spectrum $S_{out}(f)$ will be independent on gain. Instead, they will probably depend on the bias point. Assuming no other

contributions, the total output current spectrum will be

$$S_I(f) = \eta^2 S_{in}(f) + S_{out}(f) \quad (2.4)$$

Now, by measuring $S_I(f)$ for maximum gain ($\eta = \eta_{max}$) and minimum gain ($\eta = \eta_{min}$) one can deduce $S_{in}(f)$ and $S_{out}(f)$. (It can be difficult to find the bias point with $\eta = 0$). Note that it is assumed that the sources are independent on bias point, a strong assumption. Solving for the unknown contributions we get

$$S_{in}(f) = \frac{S_{I,max}(f) - S_{I,min}(f)}{\eta_{max}^2 - \eta_{min}^2} \quad (2.5)$$

$$S_{out}(f) = \frac{S_{I,min}(f) - \frac{\eta_{min}^2}{\eta_{max}^2} S_{I,max}(f)}{1 - \frac{\eta_{min}^2}{\eta_{max}^2}} \quad (2.6)$$

Eq. (2.6) appears in appended paper 2 as Eq. (1) in a frequency integrated form.

2.3.3 Phenomenological Low Frequency Noise Model

A simple low frequency noise model for the SET is now described. It does not describe the actual physical processes generating the noise, but simply assumes that there is charge and resistance fluctuations (In this sense, it is a phenomenological model). The current noise spectrum due to these sources is then calculated. Shot and quantum noise is neglected, since the magnitude of these spectra are predicted to be one or more orders of magnitude below the measured low frequency output spectra. The model was derived by A.N. Korotkov [29].

First, however, an important statement must be done: when η_{min} is small it is possible to get 2nd order, or quadratic amplification from $(\frac{\partial^2 I}{\partial Q_g^2})$. This will distort the measured spectrum, so this situation has to be avoided. In appended paper 2, the parameter $\alpha(f)$ measures the strength of the 2nd order gain. $\alpha(f)$ is defined as the convolution of the spectrum:

$$\alpha(f) = \frac{\int_{-\infty}^{\infty} S_{Q_g}(f') S_{Q_g}(f - f') df'}{e^2 S_{Q_g}(f)} \quad (2.7)$$

Next, the model is discussed. Under the assumption that the fluctuations are caused *only* by charge fluctuations and resistance fluctuations, the total current noise spectrum becomes

$$\begin{aligned} S_{I_{Q,R}}(f) = & \left(\frac{\partial I}{\partial Q_g} \right)^2 S_{Q_g}(f) + \left(\frac{\partial I}{\partial R_1} \right)^2 S_{R_1}(f) + \left(\frac{\partial I}{\partial R_2} \right)^2 S_{R_2}(f) + \\ & + K_1 \left(\frac{\partial I}{\partial Q_g} \right) \left(\frac{\partial I}{\partial R_1} \right) \sqrt{S_{Q_g}(f) S_{R_1}(f)} + \\ & + K_2 \left(\frac{\partial I}{\partial Q_g} \right) \left(\frac{\partial I}{\partial R_2} \right) \sqrt{S_{Q_g}(f) S_{R_2}(f)} \end{aligned} \quad (2.8)$$

Here, $S_{I_{Q,R}}(f)$ is the output current spectrum due to charge and resistance fluctuations. The first three terms are due to the charge fluctuations, S_{Q_g} , and resistance fluctuations, S_{R_i} in barrier 1 and 2. The two last terms models any correlation between the charge and resistance fluctuations that might exist.

The strength of the correlation is controlled by the dimensionless correlation coefficient $K_i, i = 1, 2$. Furthermore, $\frac{\partial I}{\partial Q_g}$ is the gain of the transistor, and $\frac{\partial I}{\partial R_i}, i = 1, 2$, is a measure of the current change due to a change in the resistance of junction i . For bias voltages V well above the blockade, the junction dynamic resistance is almost equal to R_i and hence, $\frac{\partial I}{\partial R_i} \approx -\frac{V}{R_i^2}$. Then, current fluctuations due to one fluctuating junction resistance becomes proportional to the square bias voltage V , $S_{I_{R_i}} = \left(\frac{V}{R_i}\right)^2 S_{R_i}$.

The following part is due to the author. Now, a rough estimate of the total resistance fluctuations, S_R can be found using Eq.(2.8). By measuring noise for low gains, it may be possible that the terms containing $S_{I_{R_i}}$ dominate the noise contribution. Then, assuming that the two junctions are identical, $K_1 = K_2 = K$, $R_1 = R_2 = R/2$, and $S_{R_1} = S_{R_2} = S_R$, Eq.(2.8) simplifies to

$$S_{I_{Q,R}}(f) = \eta^2 S_{Q_g}(f) + (\kappa_1^2 + \kappa_2^2) S_R(f) + K\eta(\kappa_1 + \kappa_2) \sqrt{S_{Q_g}(f) S_R(f)} \quad (2.9)$$

where the notation from Eqs.(1.10) and (1.14) is used. Now, assuming a constant background charge noise, $S_{Q_g} = \text{const}$ (S_{Q_g} may vary with bias), the resistance fluctuations are found to be

$$S_R(f) = \left(-\frac{\kappa_1 + \kappa_2}{\kappa_1^2 + \kappa_2^2} \frac{K}{2} \eta \sqrt{S_{Q_g}} \pm \sqrt{\frac{S_{I_{Q,R}} - \eta^2 S_{Q_g}}{\kappa_1^2 + \kappa_2^2} + \frac{\kappa_1 + \kappa_2}{\kappa_1^2 + \kappa_2^2} \frac{K^2}{4} \eta^2 S_{Q_g}} \right)^2 \quad (2.10)$$

Finally, by assuming that $\kappa_1 = \kappa_2 = \kappa$, which is true for voltages much greater than the blockade, the fluctuations become

$$S_R(f) = \left(-\frac{K\eta\sqrt{S_{Q_g}}}{2\kappa} \pm \sqrt{\frac{S_{I_{Q,R}} - \eta^2 S_{Q_g}}{2\kappa^2} + \frac{K^2\eta^2 S_{Q_g}}{4\kappa^2}} \right)^2 \quad (2.11)$$

The assumptions are strong. Nevertheless, it is at least possible to estimate the order of magnitude of S_R .

Now, a comparison between the input/output separation from the section above and a simple model is possible. The separation in Eq.(2.4) is the same as Eq.(2.9) only if there is no correlation, $K = 0$. Then, assuming that $S_{Q_g}(f) = S_{in}(f)$ one finds $S_R(f) = \frac{S_{out}}{\kappa^2}$. If $S_{Q_g}(f)$ is known, $S_R(f)$ is given by Eq.(2.11) for any correlation. The usual experimental situation is such that $S_{Q_g}(f)$ dominates and is easily determined. Then $S_R(f)$ is easily found.

Chapter 3

Experimental Techniques

3.1 Sample Fabrication

The aluminum process used by many groups to fabricate SETs is by now well established. It is based on the standard shadow evaporation technique [44, 45]. A review of the process is given in Ref. [46]. The process uses only a single e-beam lithographic step. This makes it possible to go from layout to working sample in one day. However, several weeks can be used to calibrate and fine tune the process parameters. Once the parameters are found, it is possible to mass fabricate Al SETs with a yield between 25 – 75% (depending on sample size).

Using the process, almost 50 SETs and single junctions were fabricated over a three month period. The SETs were fabricated on a *Si* substrate covered by a 1 μm *SiO_x* layer for insulation. *Au* contact pads were defined using photolithography. The e-beam resist consisted of a 300 nm bottom layer of Copolymer and a 60 nm PMMA top layer. After e-beam lithography, the pattern was developed in an isopropanol:*H₂O* mixture (10:1 by volume). Aluminum was deposited using thermal evaporation. The junction oxide was formed by letting in *O₂* into the evaporation chamber. Finally, lift-off was done in warm acetone. The resistances directly after fabrication covered a very wide range, from 500 Ω to 100 M Ω . The layouts were almost identical, but the overlap and oxidation doses varied from sample to sample. To achieve an initially low resistance, the oxidation dose was very small. The sample was oxidized for 60 seconds using *O₂* at $2.5 \cdot 10^{-3}$ mbar (The background pressure was $1 \cdot 10^{-3}$ mbar). Only a few SETs have so far been measured. The total capacitance, C_{Σ} , of these ranged between 0.2 – 0.5 fF.

After fabrication and room temperature characterization, the samples were stored in a vacuum container. However, the pressure inside the container is relatively high, typically on the order of the oxidation pressure. As a consequence, the resistance of the SETs usually increases with time. For instance, the low ohmic sample reported in appended paper 2, had 3.5 k Ω directly after fabrication (see oxidation above), but had increased to 45 k Ω six months later. This behavior offers a post trim method to increase the sample resistance after the processing.

3.2 Cryogenics

All measurements were done in an Oxford TLE200 dilution refrigerator. The base temperature is about 15 mK. The sample, mounted at the mixing chamber, is connected by 13 DC leads to the room temperature electronics. The leads are filtered with 0.5 m of Thermocoax to reduce the black body microwave radiation from parts at room temperature [27]. Furthermore, 100 pF capacitors are parallel coupled to ground to further reduce high frequency noise. The DC leads have low thermal conductance to lower the heat load on the mixing chamber. Unfortunately, this also results in low electric conductance. The total series resistance is on the order of $40\ \Omega$. Furthermore, the total line capacitance is on the order of 1 nF. This high value of capacitance together with the high value of the SET impedance, makes up a low pass filter with a cut-off frequency of order 300 Hz, using a voltage measurement setup. This explains the lack of high frequency noise experiments.

3.3 Measurement Setup

The Measurement setup used is depicted in Fig.(3.1). The main parts are the current preamplifier, the real time FFT spectrum analyzer and the measurement computer. Bias voltage was applied by a Yokogawa 7651 and then made symmetric around ground by a symmetrizer. Gate voltage and lock-in signal was applied by a Stanford DS345 synthesized function generator. To separate the analog ground from digital (GPIB) ground, isolation transformers, an optoisolator and a differential amplifier were used. Without these, line frequency harmonics from ground loops dominated the noise spectrum. The signal from the sample was amplified by the current preamplifier and then sent to the FFT analyzer. The FFT algorithm demands equally spaced frequency points. This conflicts with the tradition to present spectra with logarithmic axes. To increase the resolution, the total frequency spectrum was divided into four subspectra of 800 points each, with ranges 0-100 Hz, 0-1 kHz, 0-10 kHz and 0-100 kHz. The subspectra were afterwards merged into the total spectrum in the post analysis. The spectra were collected via GPIB by a Macintosh computer running Lab-View 3.1 software. Analysis and post processing was performed using Igor 3.1 software (which also produced most of the graphs in this thesis).

3.4 Crosstalk

Another problem with the DC leads is crosstalk. When measuring transistor noise it is necessary to measure gain in order to refer the noise to the input. Usually, this is done with a lock-in amplifier operating at a convenient frequency, say 100 Hz. Unfortunately, the crosstalk from the gate DC lead to the output DC lead is so large at this frequency that it makes it impossible to separate the gain contribution from the crosstalk. The crosstalk is mainly capacitive, and thus increases with frequency. Lowering the frequency may lower the crosstalk, but then the lock-in carrier ends up right in the frequency band of interest, blurring the noise there.

One method to determine the gain is to use the current-gate voltage (IV_g) modulation as an input signal [47]. By ramping the gate voltage, the (IV_g)

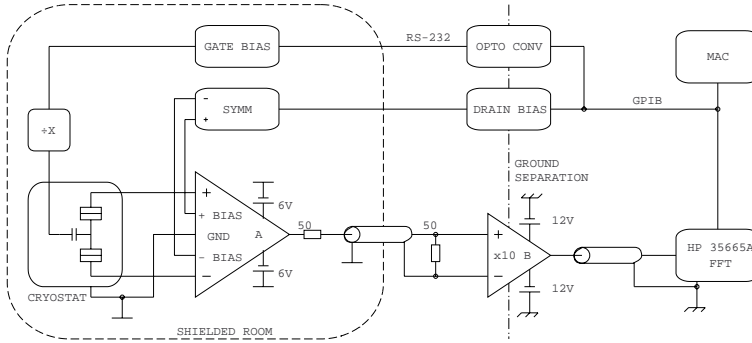


Figure 3.1: Measurement Setup. A = Differential Current Preamplifier, B = Differential Voltage Amplifier (SRS560), Gate Bias = DS345, Drain Bias = Yokogawa 7651, Symm = Symmetrizer.

modulation is used as the signal. Increasing the ramp rate then increases the frequency, and the bandwidth is found as the frequency where the modulation curve drop 3 dB in amplitude. The crosstalk from the ramp will only be an extra DC term, since the coupling is capacitive. One problem arises when the ramp switches from its maximum to minimum value. The capacitive coupling converts this into a large spike, which can saturate the amplifier. By gating the signal before the amplifier this problem can be overcome. Unfortunately, this method was too complex to be used during the noise measurements. The lock-in method was tried at 1 kHz. However, the crosstalk was too large to separate the gain. Instead, gain was determined from the modulation curves.

3.5 Current Preamplifier Review

All results presented in this thesis were obtained from measurements done with a current preamplifier. The preamp was designed, partly built and tested by the author. The primary results were presented at ISEC'97 (see appended paper 1). Below, some clarifications and extensions to this paper are given. It is worth noting that the PTB and Moscow State groups have also started using current preamplifiers [37].

3.5.1 Introduction

The current preamplifier in its most simple configuration is an Ampere meter. As such, it should accept current through its input terminals without producing a voltage drop across them, *i.e.* it must have a low series impedance. Input impedance is a figure of merit for a current preamplifier. For analog signal processing purposes, it is desirable that the preamp converts the input current to a voltage (since almost all analog signal processors are based on voltage controlled op-amps, see *e.g.* [48,49]). The transfer function, or gain should be as large as possible. The gain, defined as output voltage over input current, has the unit of impedance (Ω). Hence, such preamps are often called transimpedance

amplifiers. Finally, the output impedance of the preamp should be low, since it has a voltage output.

Current preamplifiers are used for read-out of accelerometers [50] and photodiodes [51]. An in-depth analysis of the current preamplifier is given in Ref. [51]. Although it treats photodiodes, the analysis can be applied to SETs. The results are quite technical, but are needed to explain the high frequency performance. They are reviewed below.

3.5.2 DC properties

The simplest form of a current preamplifier is shown in Fig.(3.2). It consists of an op-amp, $A1$, and resistance, R_f . The source driving the amplifier is modeled by a current source i_s in parallel with a resistance r_o (Norton equivalent model). A voltage source, V_b , is used to bias the source. The function of the circuit is simple. $A1$ has negative feedback from output to input by R_f . The feedback forces the potential at the inverting input (V_-) of $A1$ to equal that of the noninverting input (V_+), in this case V_b . Whatever current that is passed through R_f , the op amp will adjust its output voltage, V_{out} so that V_- equals V_b . The output voltage will then be the sum of V_b and the voltage drop across R_f , which is proportional to the input current.

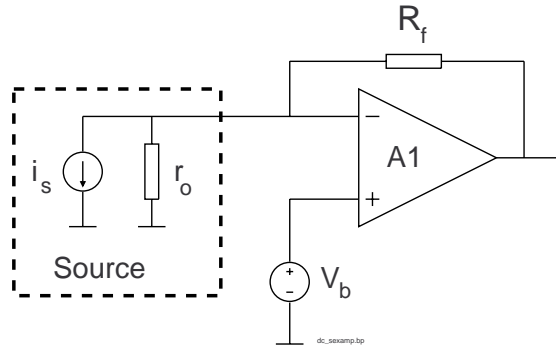


Figure 3.2: Basic current preamplifier. The amplifier consists of an op amp, $A1$, and a feedback resistor R_f . The source shown, is connected to the inverting input of $A1$ and is modeled with its Norton equivalent circuit. The feedback loop will voltage bias the source so that $V_- = V_+ = V_b$.

A more realistic DC model for the op amp is shown in Fig.(3.3). Offset voltage and bias current errors of the op amp are now included. The input impedance of the op amp is neglected, since it is relevant only when it is less than R_f . In a good design this is never the case. Furthermore, the output impedance can be made unimportant by connecting a voltage follower after the preamp. The DC properties of interest are: gain, input impedance, bias accuracy and total output voltage. Below, several approximations are made in the equations. These are validated by using experimental numbers for several parameters. In the experiments, the op amp AD743JN from Analog Devices, Inc. was used [50]. Vital data for the op amp are given in Table (3.1). The feedback resistance was

Offset Voltage	V_{os}	0.25 mV
Bias Current	I_b	190 pA
DC Open Loop Gain	A_O	$4 \cdot 10^6$
Differential Input Resistance	R_{dm}	$10^{10} \Omega$
Total Input Capacitance	C_{in}	38 pF
Unity Gain Frequency	UGF	4.5 MHz
Gain Bandwidth Product	GBW	4.5 MHz
Input Equivalent Voltage Noise	e_n	$3.2 \text{ nV}/\sqrt{\text{Hz}}$ @ 1 kHz
Input Equivalent Current Noise	i_n	$6.9 \text{ fA}/\sqrt{\text{Hz}}$ @ 1 kHz

Table 3.1: AD743JN typical data used in the text. Supply voltage = $\pm 15 \text{ V}$, $T = +25^\circ \text{C}$.

$R_f = 10 \text{ M}\Omega$ while the SET output impedance was $r_o \geq 20 \text{ k}\Omega$.

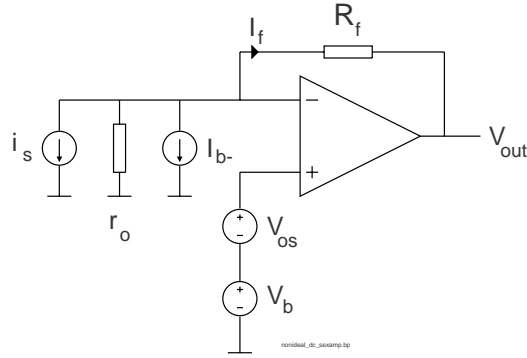


Figure 3.3: Current preamp with DC error sources of the op amp included. V_{os} is the input offset voltage. I_{b-} is the input bias current of the inverting input.

The DC gain is the ratio of the output voltage to the input current, with an ideal current source connected (*i.e.* $r_o = \infty$). The gain is

$$G \equiv \frac{V_{out}}{I_f} = R_f \frac{A_O}{1 + A_O} \approx R_f = 10 \text{ M}\Omega \quad (3.1)$$

where A_O is the open loop DC gain of the op amp. A high gain means choosing a high R_f and A_O . Any real source will have a finite output resistance, which will shunt the preamp. Hence, the preamp should have as low input impedance as possible. This is given by

$$R_{in} \equiv \frac{V_-}{I_f} = \frac{R_f}{1 + A_O} \approx \frac{R_f}{A_O} = 10 \Omega \quad (3.2)$$

Finally, the bias voltage accuracy is how good V_- follows V_+ ($= V_b$). Calculations yield

$$V_- = V_b + V_{os} + \frac{I_f R_f}{A_O} \approx V_b + V_{os} \quad (3.3)$$

For high accuracy, V_{os} should be minimized and A_O should again be maximized. By combining the effects of source and input impedance, bias current and gain above, the total output voltage (V_{out}) becomes

$$V_{out} = V_b + V_{os} + (i_s + I_{b-}) \left(\frac{1 + A_O}{1 + A_O + \frac{R_f}{r_o}} \right) R_f \approx V_b + V_{os} + (i_s + I_{b-}) R_f \quad (3.4)$$

From Eqs.(3.4) and (3.3), one finds that the bias point is translated from the desired point by the op amp error sources. Note that the bias voltage V_b has to be subtracted to get the current reading.

3.5.3 AC properties

For finite frequencies, reactive components must be included. This is shown in Fig.(3.4). Here, C_{tot} is the total capacitance at the negative node, and is $C_{tot} = C_l + C_{op}$, where C_{op} is the op amp capacitance. In the experiments, $C_l \approx 1$ nF, whereas for the AD743, $C_{op} \approx 40$ pF. Thus, $C_{tot} \approx C_l \approx 1$ nF. Parallel with R_f is a capacitor C_f . Since very high resistances are used for R_f (≥ 1 M Ω), very small values of C_f will affect circuit performance. It is therefore necessary to include parasitic capacitances into C_f . (For instance, a resistor has a parallel capacitance on order 0.5 pF). At frequencies above a few Hz, the gain

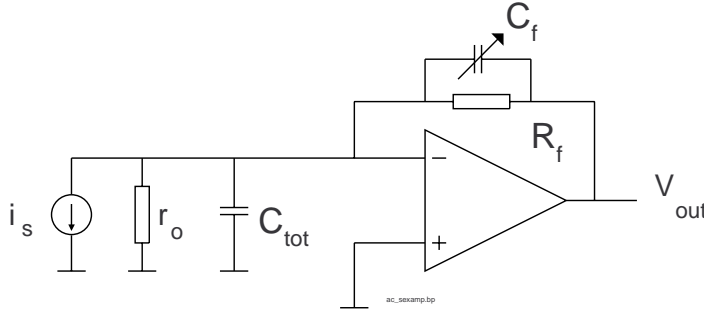


Figure 3.4: The current preamplifier with reactive components C_{tot} and C_f included. The gain of the op amp is frequency dependent which also has to be included into the calculations.

of the op amp starts to roll off at -20 dB/decade. This has to be included into the calculations. To a first approximation, the open-loop gain of the op amp is

$$A_{OL}(\omega) = \frac{A_O}{1 + j\omega/\omega_0} \quad (3.5)$$

where, $\omega_0 \equiv \frac{2\pi GBW}{A_O}$ and GBW is the gain bandwidth product of the op amp. As a consequence, A_O has to be replaced by $A_{OL}(\omega)$ in all the equations above.

The AC gain is set by the feedback impedance $Z_f = R_f \parallel C_f$. Using Eq. (3.1) yields

$$G(\omega) = \frac{R_f}{1 + j\omega R_f C_f} \quad (3.6)$$

which is the DC gain multiplied by a low pass transfer function with cut-off frequency $\omega_f = 1/R_f C_f$. Typical values are $C_f \approx 2 - 20$ pF, which yields frequencies of $f_f \equiv \frac{\omega_f}{2\pi} \approx 0.8 - 8$ kHz. This is the bandwidth obtainable with a *perfect* current source. This is not the case in the experiments. The source is shunted by the parallel combination of C_l and r_o . As the frequency increases, so does the shunting by C_l . To calculate the bandwidth, the AC input impedance of the preamp must be known. Calculations yield

$$Z_{in} = \frac{R_f \parallel C_f}{A_{OL}(\omega)} = \frac{R_f}{A_O} \frac{1 + j\omega/\omega_0}{1 + j\omega/\omega_f} \quad (3.7)$$

For most cases, $\omega_0 \ll \omega_f$. The resulting input impedance is sketched in Fig. (3.5). The impedance has two break frequencies, ω_0 and ω_f . For $\omega \ll \omega_0$, $Z_{in} = R_{in} = \frac{R_f}{A_O}$ and is resistive and equal to the DC input impedance. For $\omega_0 \ll \omega \ll \omega_f$, $Z_{in} = j\omega(\frac{R_f}{A_O \omega_0}) \equiv j\omega L_{eq}$ and is inductive. The equivalent inductance in the experiments becomes $L_{eq} = 0.36$ H, a very large value. When $\omega \gg \omega_f$, $Z_{in} = 1/(A_O \omega_0 C_f)$, which is resistive. Also, the gain starts to drop in this frequency region.

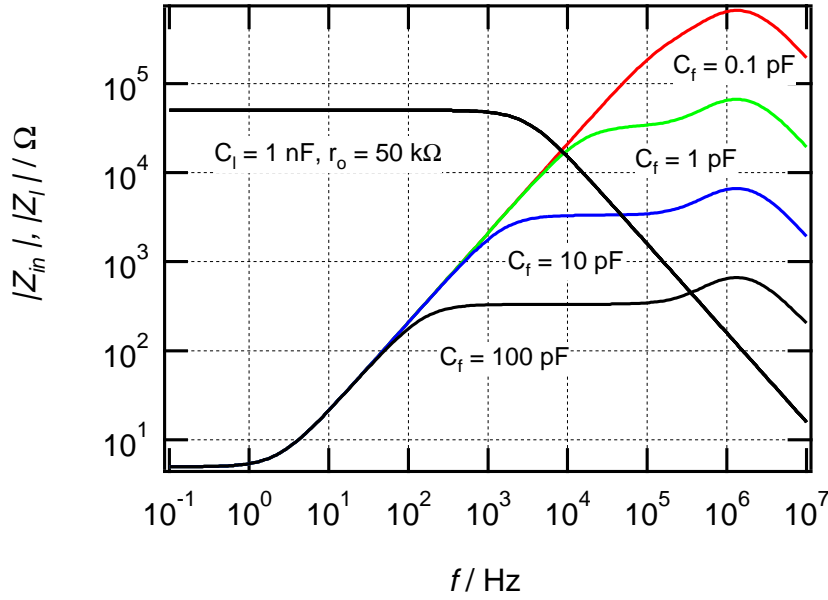


Figure 3.5: SPICE [52] simulation of the circuit in Fig.(3.4) shows the input impedance of the amplifier, $|Z_{in}|$, and the source impedance $|Z_l|$. Experimental values used are found in the text. Note the bulges in $|Z_{in}|$ at $f = 1$ MHz. The cause of these are a second pole in the op amp gain, not included in Eq.(3.5).

The bandwidth of the total system, ω_s , can now be estimated. At high frequencies, the source current divides between the line capacitance C_l and the preamp input impedance, Z_{in} . At some frequency, ω_g , exactly half the current is passed through C_l and Z_{in} each. If this happens in the inductive region of

Z_{in} , then the frequency is found by equating $|X_{C_l}|$ to $|Z_{in}|$:

$$\frac{1}{\omega_g C_l} = \omega_g \left(\frac{R_f}{A_{OL} \omega_0} \right) \Rightarrow \omega_g = \sqrt{\frac{A_{OL} \omega_0}{R_f C_l}} \Rightarrow f_g = \sqrt{\frac{GBW}{2\pi R_f C_l}} \quad (3.8)$$

The final form in Eq.(3.8) is Eq.(1) in appended paper 1. This is then the system bandwidth ω_s . This situation corresponds to the $C_f = 0.1$ pF curve in Fig.(3.4). However, if the source impedance is low enough that the crossing frequency occurs in the high frequency region of Z_{in} , the bandwidth is simply set by the transimpedance network, from Eq.(3.6) above

$$f_g = \frac{1}{2\pi R_f C_f} \quad (3.9)$$

This corresponds to the $C_f = 10$ pF curve in Fig.(3.4).

By combining the current division and the gain, the total AC transfer function can be calculated:

$$Z_T(\omega) = \frac{R_f}{1 - \omega^2 C_l L_{eq} + j\omega(1/\omega_f + R_{in} C_l + L_{eq}/r_o + 1/(2\pi GBW))} \quad (3.10)$$

This equation is valid for all frequencies of interest. It breaks down somewhere close to $f = GBW \approx 4.5$ MHz, due to high frequency poles neglected in the op amp open loop gain, Eq.(3.5). Note the resonance formed by the inductance L_{eq} and C_l . It is this resonance that causes ringing and sometimes oscillations, (see also Sec.(3.5.5)). An example of Eq.(3.4) is shown in Fig.(3.6). Note also that Eq.(3.4) has the same form as a second order low pass filter with DC gain R_f (see Ref. [53]).

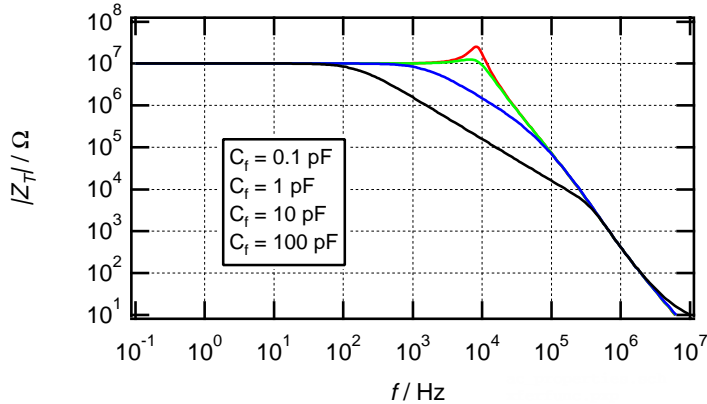


Figure 3.6: SPICE simulation of the transfer function, $|Z_T|$ for different feedback capacitances C_f . For low values of C_f , the transfer function has a resonance, which originates from the interaction of the source capacitance C_l and the input inductance L_{eq} of the preamp.

It is interesting to note that the bandwidth is quite insensitive to the source impedance, r_o . This is due to C_l which shunts r_o at high frequencies. In a voltage

amplifier, the total bandwidth is set by $f_g = 1/2\pi R_f \parallel C_l$ and varies between $f_{g,min} = 1/2\pi R_f C_l$ and $f_{g,max} = 1/2\pi r_o, min C_l$. The voltage preamplifier bandwidth is inversely proportional to r_o whereas the current preamplifier is almost independent of r_o . This is a clear advantage of the current preamplifier.

3.5.4 Noise Properties

The noise performance of the current preamplifier is analyzed with the help of Fig.(3.7). Here, noise sources for the op amp and the feedback resistor have been included. The goal is now to calculate the input referred noise current for the system. This is done in two steps. First, the contribution of all sources are calculated at the output of the preamp. Then, this total output noise is input referred by dividing it with the transfer function from Eq.(3.10). The output

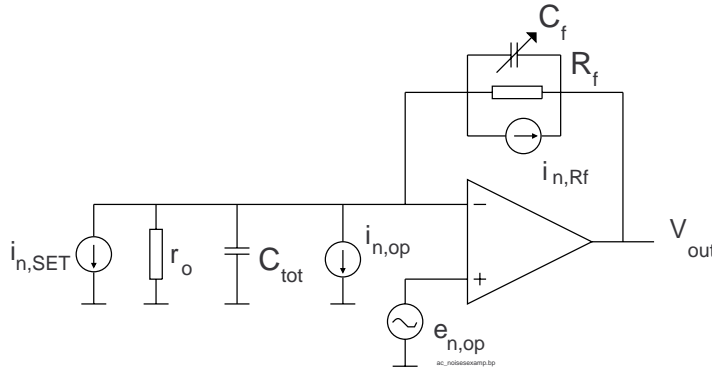


Figure 3.7: The current preamplifier with noise sources included. $i_{n,op}$ and $e_{n,op}$ are the current and voltage noise sources of the op amp, respectively. i_{n,R_f} is the thermal noise of the feedback resistor R_f .

contributions of the current noise sources $i_{n,op}$ and i_{n,R_f} are easily calculated. By inspection, $i_{n,op}$ is parallel to the SET source $i_{n,SET}$. Furthermore, i_{n,R_f} is also in parallel with $i_{n,SET}$, since its right leg is grounded by the op amp output. Hence, the sources $i_{n,SET}$, $i_{n,op}$ and i_{n,R_f} all have the same transfer function, given by Eq.(3.10). Next, the contribution of the op amp noise voltage, $e_{n,op}$ is calculated and yields

$$e_{out} = \left(\frac{1}{R_f} + \frac{1}{r_o} + j\omega(C_l + C_f) \right) Z_T(\omega) e_{n,op} \quad (3.11)$$

Note the so called noise-rise term, $j\omega(C_l + C_f)e_{n,op}$. This seriously limits the high frequency noise performance of the preamp.

The total output noise voltage is found by summing all contributions, since all sources are uncorrelated. Furthermore, since all terms in the sum contains the common factor $Z_T(\omega)$, the input current noise is obtained directly by division by $Z_T(\omega)$, yielding

$$i_{in}^2 = i_{n,SET}^2 + \frac{4k_B T}{R_f} + i_{n,op}^2 + \left(\frac{1}{R_f} + \frac{1}{r_o} + j\omega(C_l + C_f) \right)^2 e_{n,op}^2 \quad (3.12)$$

where $i_{n,R_f} = \frac{4k_B T}{R_f}$ is the Johnson noise of the feedback resistor. Thus, to measure SET noise, $i_{n,SET}^2$ must be greater than the sum of the other terms in Eq.(3.12). The low frequency noise floor is set by R_f , and this was the main criterion for selecting the feedback resistance.

An important question is if it possible to detect shot noise of the SET. This is given by $i_n = \sqrt{2eI}$, where I is the bias current. At high frequencies, the noise rise term of the current preamplifier dominates, and the input current noise is given by $i_n = e_n 2\pi f C_l$. By equating the noise terms, an upper frequency where the contributions are equal is found. Solving for the frequency yields

$$f = \frac{\sqrt{2eI}}{2\pi e_n C_l} \quad (3.13)$$

Assuming $I = 1$ nA and using experimental values gives $f = 0.95$ kHz. In this region, all SETs are dominated by $1/f$ noise, and it is not possible to detect shot noise. Either a higher current or a lower $e_n C_l$ product is needed.

3.5.5 Stability

Instabilities are very likely to occur in the current preamplifier. These manifest themselves as excessive ringing or even oscillations of the preamp. The cause of the oscillations is the feedback. Any feedbacked system is a potential oscillator. Usually, to get more insight in what's going on, the open loop noise gain is studied [51]. It is the noise that starts the oscillation. (The closed loop noise gain is given by Eq.(3.11)). The cause of the instability is the combination of two poles in the open loop gain. The first pole is from the op amp open loop gain, Eq.(3.5). The second is formed by R_f and C_l . Together, they give 180 degrees phase lag at frequencies where the loop gain is greater than unity, causing oscillation. The remedy is to connect a feedback capacitor across R_f . By choosing it appropriately, it will give enough phase lead to make the system stable. However, this will lower the gain of the preamp, see Eq.(3.6). Thus, there is a trade-off between gain and stability. The optimum value of C_f is given by

$$C_f = \frac{C_c}{2} \left(1 + \sqrt{1 + \frac{4C_l}{C_c}} \right), C_c = \frac{1}{2\pi R_f GBW} \quad (3.14)$$

This gives a phase margin of 45 degrees, yielding a slightly peaked gain. Note that C_f is a function of the two poles (via C_c) discussed above. C_f is approximately proportional to the inverse square of R_f and GBW. With the experimental values, this gives $C_f \approx 3.8$ pF. This value is so small that parasitic capacitances from the board layout and feedback resistor will change the effective C_f from the value installed. It is therefore wise to install a tunable capacitor (2 – 20 pF range) instead of a fixed value. This also accommodates lower feedback resistors.

Note that the equation above is derived without a source resistance r_o . However, the inclusion of r_o will only lower the feedback, making the preamp more stable (*i.e.* a shorted input results in no feedback at any frequency, removing the cause of oscillations).

It is recommended that the op amp used is unity gain stable. Even though the noise gain increases above unity at high frequencies (where it matters), the high capacitive load (C_l) makes non-unity gain amplifiers very difficult to

compensate. This is also a consequence of the fact that the impedance at the input of the preamp is much more complex than the model used here, *i.e.*, C_l . This complicates the stability prediction. A tunable C_f is highly recommended. Often, the bandwidth then decreases so much that the initially high bandwidth is sacrificed by the compensation. Thus, there is no increase in bandwidth.

3.5.6 Differential Current Preamplifier

External sources will induce noise in the preamp. Due to the long measurement leads from sample to preamp used in cryostats, noise pick-up could spoil the signal to noise ratio. By using a differential preamplifier [51], the external noise can be minimized. Such an amplifier is shown in Fig. (3.8). The main function is that the output voltage is the *difference* of the inverting current and the non-inverting current. The current source will pull current out of the inverting input and push the same current into the non-inverting input. The output voltage will then be $2R_f i_s$. An external signal will induce equal amounts of noise into the inverting and noninverting inputs. The difference will then be zero. It is

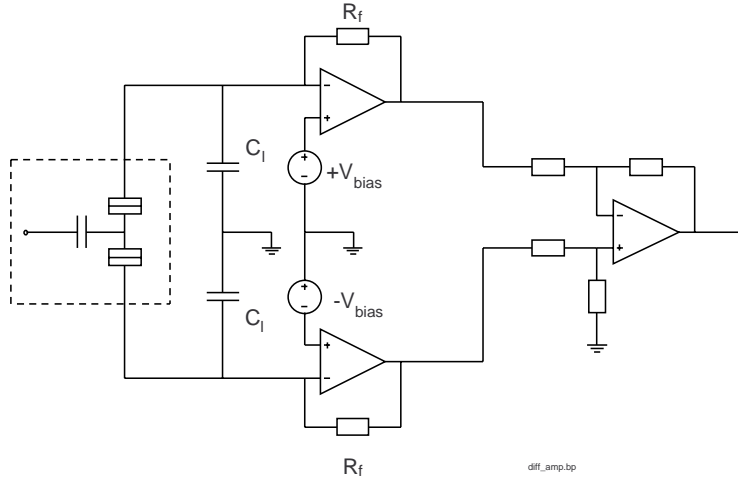


Figure 3.8: Differential Current Preamplifier. R_f = feedback resistors, C_l = line capacitance, $\pm V_{bias}$ = bias voltage.

easy to generalize the single-ended current preamplifier result. First, the gain, Eq.(3.10), will be doubled, since the signal current now passes through two feedback resistors. Second, the input noise current, Eq.(3.12) will be halved. The most important characteristics are given below. Note that the output voltage still includes the bias voltage, V_b , and has to be subtracted to give a true current reading.

$$V_{1-} = V_b/2 + V_{os,1} \quad (3.15)$$

$$V_{2-} = -V_b/2 + V_{os,2} \quad (3.16)$$

$$V_{out} = 2Z_T i_s + (V_{1-} - V_{2-}) \quad (3.17)$$

$$i_{in}^2 = i_{n,SET}^2 + \frac{2k_B T}{R_f} + \frac{i_{n,op}^2}{2} + \left(\frac{1}{R_f} + \frac{1}{r_o} + j\omega(C_l + C_f) \right)^2 \frac{e^2}{2} \quad (3.18)$$

3.5.7 Voltage Bias Precautions

Standard practice when handling samples in the cryostat is to ground all measurement leads when they are not used. This is for protection against electrostatic discharge. This practice is compatible with a passive bias setup, at Chalmers called "R-bias". What might not be so obvious is that sample grounding is *not* compatible with a voltage bias ("V-bias") setup. Some users have had their samples destroyed when opening the ground shorts in V-bias mode. This is not so strange however: when the sample is shorted, the measurement electronics is trying to voltage bias a short cut. It does this by pushing as much current as possible through the ground short, hoping to raise the potential. The consequence is that the output of the op amps usually saturates at one of the supply rails, typically $\pm 5V$. When the short is removed and the op amps have saturated at opposite rails, there is temporarily 10 volts across the two feedback resistors in series with the sample. The op amps quickly settle towards the applied bias voltage, but it might be too slow. This is of course a very unfavorable condition. The correct procedure is to *first* disconnect the sample from the preamp, and *then* ground the sample.

Chapter 4

Results

4.1 Preamplifier Performance

The transimpedance amplifier was characterized using two different op amps. To get a wide bandwidth, low noise high speed op amps, (OPA655 from Burr-Brown) were installed. Such an amplifier has a GBW of 240 MHz and FET inputs, making it compatible with high impedance sources *i.e.* SETs. To optimize bandwidth further, low feedback resistors (820 k Ω) were used. Together with the DC line impedance of $C_l \approx 1$ nF, this implies a bandwidth of $f \approx 216$ kHz. However, the preamplifier was not stable and feedback capacitors had to be installed (See Sec.(3.5.5)). After stability tuning, the bandwidth was checked with a SET connected. To reduce crosstalk, the method described in Sec.(3.4) was used. The resulting bandwidth was found to be very low, $f \approx 6.2$ kHz. However, it was still much higher than the usual resistive bias/voltage measurement setup. A bandwidth comparison of the two methods is shown in Fig.(4.1(a)). These results together with some preliminary noise data on a SET were pre-

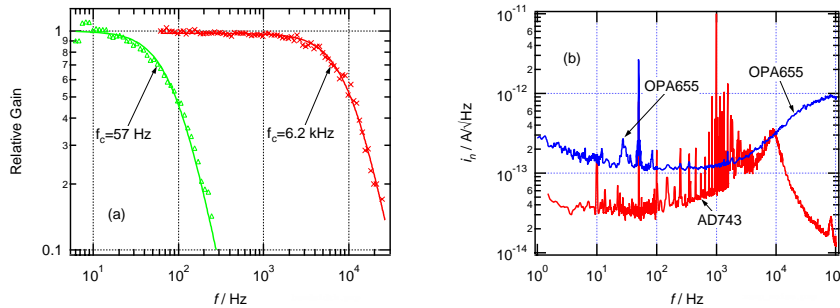


Figure 4.1: (a). Voltage (Δ) and current (X) preamplifier bandwidth using the high ohmic SET in the normal state. Data acquired at $T = 30$ mK and $B = 1.0$ T. (b). Noise performance for OPA655 (upper curve) and AD743 (lower curve). The peaks around 1 kHz in the lower curve are due to the lock-in signal and mechanical resonances within the cryostat.

sented at *ISEC'97* and are enclosed as appended paper 1. The reason for the low bandwidth is that the line capacitance is very high, making it very diffi-

cult to achieve stability at high frequencies. Thus, it is not the GBW of the op amp that limits the bandwidth. Rather, the large line capacitance and the feedback resistance make the amplifier very unstable, demanding a large stabilizing feedback capacitance, C_f , and the bandwidth is now set by Eq.(3.9). As a consequence, a moderate speed op amp will give the same bandwidth as high speed op amps. Using Eq.(3.8), the same bandwidth can be achieved with a 200 kHz GBW op amp, three orders of magnitude lower than the OPA655! The use of high speed op amps has other drawbacks. First of all, being devices optimized for high speed, the DC performance is much worse compared to precision DC op amps. The offset voltage has both much higher magnitude and temperature drift. Furthermore, the OPA655 has a high $1/f$ noise voltage component, which can mask the SET noise. Therefore, the high speed op amps were abandoned and an ultra low noise, precision op amp was used; the AD743. It has a GBW of 4.5 MHz, much lower $1/f$ noise, offset voltage and drift. The bias currents are comparable. Furthermore, since the GBW of 4.5 MHz \gg 200 kHz allowed by C_l , the feedback resistors were increased to 10 M Ω to lower noise without sacrificing bandwidth. The resulting noise performance is shown in Fig.(4.1(b)).

Comparing the noise performances of the different op amps, it is evident that the AD743 has a superior noise performance for *all* frequencies. Another benefit is that the power consumption of the AD743 is one third of the OPA655, an important consideration when using battery supplies. In the first appended paper, it was claimed that the bandwidth could be increased above $f \approx 6.2$ kHz. While this certainly is possible, the noise rise term in Eq.(3.11) will add so much extra noise, that the total signal-to-ratio becomes very low. The SET noise will be masked by noise, and thus there is little meaning doing this.

4.2 SET Results

Several SETs have been characterized with the preamplifier. The data presented in the appended articles is from experiments with three different SETs. The first two were $Al/Al_2O_3/Al$ devices, fabricated by the author, while the third was an $Al/AlO_x/Nb$ SET fabricated by T. Henning. The results reviewed here are from the first two devices. The data of the third device found in appended papers 2 and 3, will be discussed elsewhere.

4.2.1 High Ohmic SET

The results of the first SET were published at *ISEC'97* (see appended paper 1). This device was the first to be tested with the preamplifier. The current-voltage (IV) characteristics for several gate biases are found in Fig.(4.2(a)). From these, an asymptotic resistance of $R_N \approx 415$ k Ω and an island capacitance of $C_\Sigma \approx 145$ aF were found. To extract the capacitance, the offset method described in Ref. [54] was used. The current-gate charge (IQ) characteristics, are shown for some bias voltages in Fig.(4.2(b)). The periodic behavior of the current vs. gate charge is clearly seen. The gate charge was induced with a gate voltage. From the periodicity, the gate capacitance was deduced and was $C_g \approx 5.3$ aF. The maximum gain was $\eta_{max} = 3.2$ nA/e at a bias of $V = 1.23$ mV.

While this SET showed a well pronounced blockade, the resistance was quite high. This resulted in a low current of the device, and hence a low output signal.

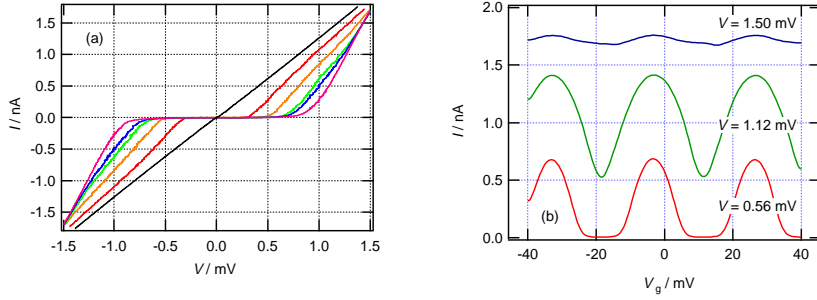


Figure 4.2: (a). IV characteristics for the high ohmic SET in the normal state. Data acquired at $T = 30$ mK and $B = 1.0$ T. (b). Gate response for the SET in (a).

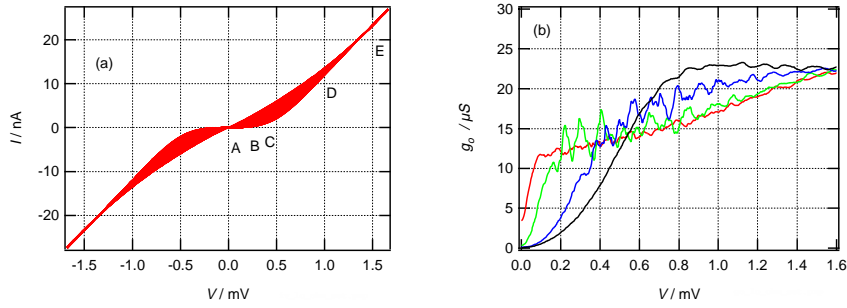


Figure 4.3: (a). IV characteristics for the low ohmic SET in the normal state. Data acquired at $T = 30$ mK and $B = 0.15$ T for many gate biases. Points A to E marks bias voltages where noise was measured. (b). Output conductance $1/r_o$ for the SET in (a). From left to right, $Q_g = 0$, $Q_g = e/6$, $Q_g = e/3$ and $Q_g = e/2$.

Also, the OPA655 added much noise, making it difficult to measure the SET noise with high accuracy.

4.2.2 Low Ohmic SET - Normal State

The results of the low ohmic SET is to be published in the second appended paper. The data were acquired using AD743 op amps. The IV characteristics are shown in Fig.(4.3 (a)). This device had a low asymptotic resistance of $R_N \approx 45$ k Ω , while the island capacitance was $C_\Sigma \approx 190$ aF. Due to the low resistance, the cotunneling is large and the blockade is smeared to a greater extent than the high ohmic SET. A comparison of the two SETs is shown in Fig.(1.2). The current scale is much greater for the low ohmic SET, allowing a larger signal and better accuracy than for the larger resistance one. The output impedance of the device, r_o , is shown in Fig.(4.3 (b)), and was always above 40 k Ω . This parameter was needed for the noise analysis, see below. The gate response is shown in Fig.(4.4 (a)). The maximum modulation was $\Delta I \approx 3.9$ nA at a bias $V = 0.53$ mV. Thus, this transistor has a much higher current response

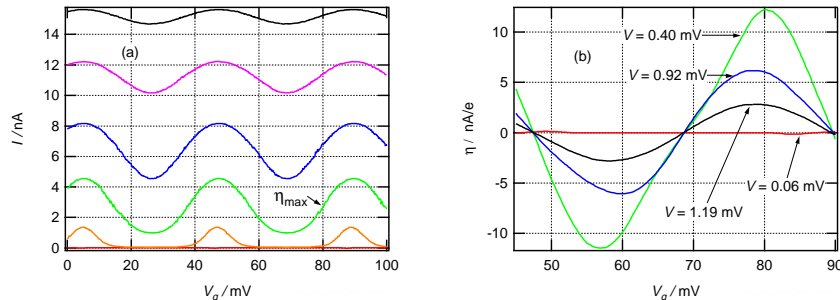


Figure 4.4: (a). Normal conducting gate response for the low ohmic SET for several bias voltages. From the bottom, $V = 0.06$ mV, $V = 0.13$ mV, $V = 0.40$ mV, $V = 0.66$ mV, $V = 0.92$ mV and $V = 1.19$ mV. η_{max} is the maximum gain bias point. (b). Gain, η , vs. gate bias for several bias voltages.

compared to the high ohmic device even though it has a smeared blockade. As a consequence, the maximum gain, $\eta_{max} \approx 12$ nA/e, found at $V = 0.40$ mV, is almost four times higher. The maximum gain bias point is marked in the curves below. The gain is shown in Fig.(4.4 (b)). This is the expected result from the discussion in Sec.(1.2.2). Even though the charging energy is 33 % higher in the high ohmic SET, it's high impedance lowers the current scale.

4.2.3 Low Ohmic SET - Superconducting State

IV characteristics were also recorded in the superconducting state, and are displayed in Fig.(4.5 (a)). The superconducting gap is clearly visible. Since no supercurrent was detected, the Josephson Coupling Energy, E_J , was small. The output impedance, r_o , is displayed in Fig.(4.5 (b)). It is very high in the gap (as expected) and drops dramatically for bias voltages above the gap. Note that $r_o < R_N$. This is due to the singularity in the density of states of the electron states in a superconductor [55]. This low impedance may limit the noise performance of the preamplifier, see Eq.(3.12).

On the other hand does this singularity give a very high current modulation, as found in Fig.(4.6 (a)). The maximum modulation, $\Delta I_{max} \approx 7.8$ nA is found close to the gap at $V = 0.82$ mV. It is also visible in the IV curves. The gate *voltage* periodicity of the current modulation was the same as in the normal state, which again tells us that the current mainly consists of single electrons and not Cooper pairs. The gain is shown in Fig.(4.6 (b)). The maximum gain, $\eta_{max} = 34$ nA/e, was found at $V = 0.84$ mV. This is almost three times higher than the maximum normal state gain. This clearly shows the gain advantage of a superconducting SET compared to a normal conducting SET.

4.2.4 Superconducting and Normal SET Noise Spectra

Over 130 noise spectra were recorded for the low ohmic SET in the normal state, and 25 in the superconducting state. The spectra were gathered for five different bias voltages, and 26 gate biases (in the normal state) or five gate biases (in the superconducting state). In this subsection, the lowest noise performance

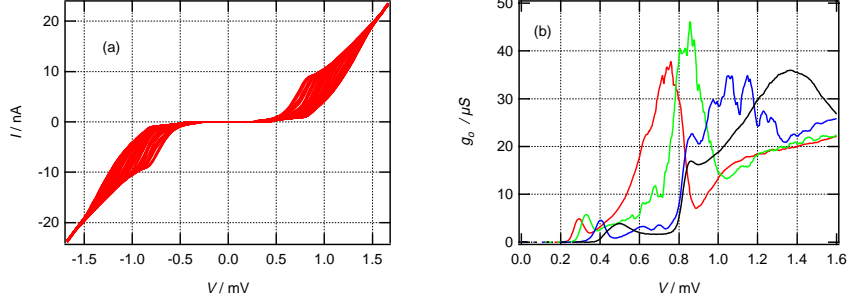


Figure 4.5: (a). IV characteristics for the low ohmic SET in the superconducting state for several gate biases. Data acquired at $T = 30$ mK. (b). Output conductance g_o for the low ohmic SET in the superconducting state. From left to right, $Q_g = 0, Q_g = e/6, Q_g = e/3$ and $Q_g = e/2$. Note that the maximal g_o is well above $1/R_N \approx 22\mu$ S.

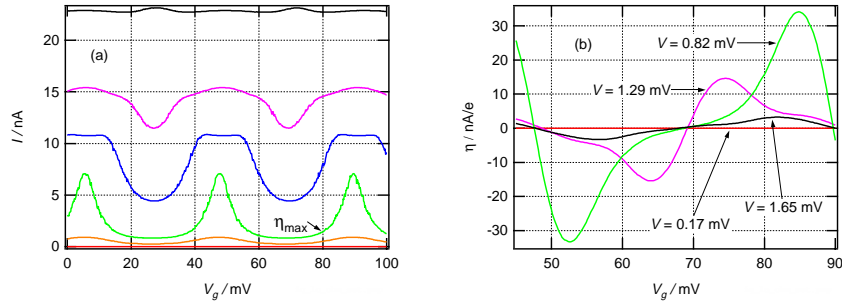


Figure 4.6: (a). Superconducting gate response for the low ohmic SET for some bias voltages. From the bottom, $V = 0.18$ mV, $V = 0.49$ mV, $V = 0.78$ mV, $V = 1.02$ mV, $V = 1.29$ mV and $V = 1.65$ mV. η_{max} is the maximum gain bias point. (b). Gain, η , vs. gate bias, for some bias voltages.

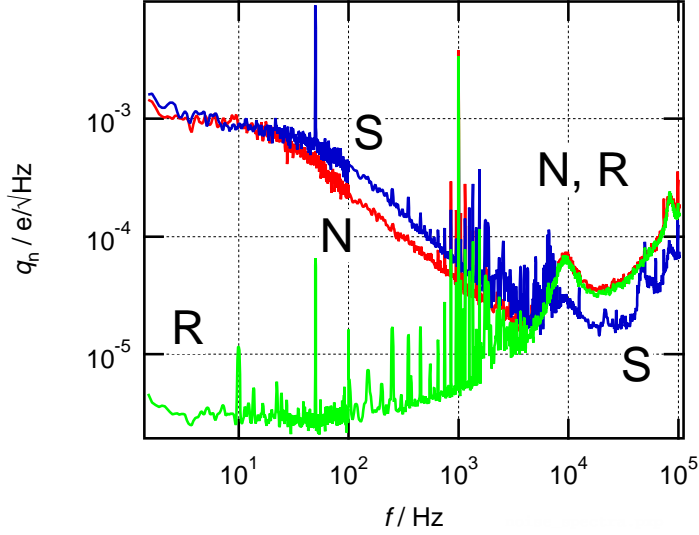


Figure 4.7: Noise spectra for the normal (N) and superconducting (S) states, respectively. The spectra were recorded at the bias points where the gain was maximum, $\eta = \eta_{max}$. For reference, the preamplifier noise spectrum (R), has been input referred to the gate of the SET, by dividing with the maximum gain for the normal state.

of the different states are reviewed. A detailed investigation of the low frequency noise was presented in appended paper 2 and is reviewed in the subsection below.

The high frequency charge noise spectra for maximum gain bias are shown in Fig.(4.7). Both normal and superconducting state operation is included. The spectra have been input referred by dividing by the frequency dependent transfer function from Eq.(3.10) and then by the charge gain, η . The frequency dependent transfer function was not measured during this experiment, since the measurement system became too complex to include all extra equipment. Instead, the gain was found from SPICE [52] simulations. This resulted in an accuracy problem for frequencies above 600 Hz. Around the preamplifier resonant frequency, the gain becomes quite sensitive to the chosen value of C_f , and the accuracy is low. A 10% gain error bar or less is achieved below $f = 600$ Hz for $C_f \leq 3$ pF and $r_o \geq 20$ k Ω , which are reasonable values. (The bandwidth was probably larger than this, since the slope of the SET noise output spectra did change until around $f = 4$ kHz).

A cross-over from input to output dominated noise behavior was found in the frequency range $1 \text{ kHz} \leq f \leq 10 \text{ kHz}$. Below 1 kHz, normal state operation shows the lowest noise, while above 10 kHz, superconducting operation had lower noise. This is due to the larger gain in the superconducting state. The noise figures were $q_n \approx 2 \cdot 10^{-5} e/\sqrt{\text{Hz}}$ at $f = 4.5$ kHz for both transistors, which is the lowest achieved together with the RF-SET. From a *charge* noise point of view, it (almost) doesn't matter if the SET is normal or superconducting since the noise is almost the same. From an *output* noise point of view, however, the superconducting state is preferable. The output noise is higher for the super-

conducting SET. Since the preamplifier noise should be compared to the output noise, this means that the preamplifier can be noisier in the superconducting state. Note also that the dynamic range (*i.e.* SET to preamplifier noise ratio) is more than 100 for low frequencies.

4.2.5 Low Frequency Noise

For frequencies below 100 Hz, the gain was flat and determined only by the feedback resistors, $Z_T = 20 \text{ M}\Omega$. In order to try to separate different contributions as described in Sec.(2.3.2), noise was measured for over 130 bias points. 26 gate biases per charge period were measured, with five different bias voltages. The SET was normal conducting, and the temperature was 30 mK. Due to the long time to record noise spectra for the lowest frequency band, $0 \leq f \leq 100 \text{ Hz}$, only 25 spectra were recorded in this band. This gave an initial accuracy of 20 %. The accuracy was then increased by integrating each current spectrum in the band $51 \leq f \leq 99 \text{ Hz}$. The limits were chosen so as not to coincide with power line harmonics. Each bias point spectrum was then represented by a single RMS current, δI_n . The spectral variables $S_{in}(f)$, $S_{out}(f)$, $S_{Q_g}(f)$ and $S_R(f)$ were also integrated into single numbers which are defined below.

$$\delta I_n = \sqrt{\int_{f_l}^{f_u} S_I(f) df} \quad (4.1)$$

$$\delta Q_{in} = \sqrt{\int_{f_l}^{f_u} S_{in}(f) df} \quad (4.2)$$

$$\delta I_{out} = \sqrt{\int_{f_l}^{f_u} S_{out}(f) df} \quad (4.3)$$

$$\delta Q_{q,n} = \sqrt{\int_{f_l}^{f_u} S_{Q_g}(f) df} \quad (4.4)$$

$$\delta R_n = \sqrt{\int_{f_l}^{f_u} S_R(f) df} \quad (4.5)$$

$$(4.6)$$

where $f_l = 51 \text{ Hz}$ and $f_u = 99 \text{ Hz}$. (In paper 2, $I_{N,exc}$ was used instead of δI_{out} . $1/f$ -noise is sometimes referred to as excess noise, while in paper 2, excess noise was defined as the remaining noise after input noise subtraction. To avoid a confusion, a change of name was necessary. Also, δR was changed to δR_n)

To see if the SET was charge or resistance noise dominated, δI_N was compared to the SET gain η . η was found by differentiation of the IQ -curves. The only fitting parameter was the gate charge. The result is shown in Fig.(4.8). Since the curves follow each other almost perfectly, it is clear that the noise in the SET is dominated by a large charge noise with a magnitude of $\delta Q_{in} \approx 2 \cdot 10^{-3} e_{RMS}$ for the (B,C, and D) bias voltages. Only for the lowest and highest bias voltage does the charge noise change. This is shown in Fig.(4.9). The input referred charge noise was $\delta Q_{in} \approx 1 \cdot 10^{-3} e_{RMS}$ for the lowest bias voltage, then increased to $\delta Q_{in} \approx 2 \cdot 10^{-3} e_{RMS}$, where it stayed approximately constant until the highest bias point, where δQ_{in} increased. The low and high values of the

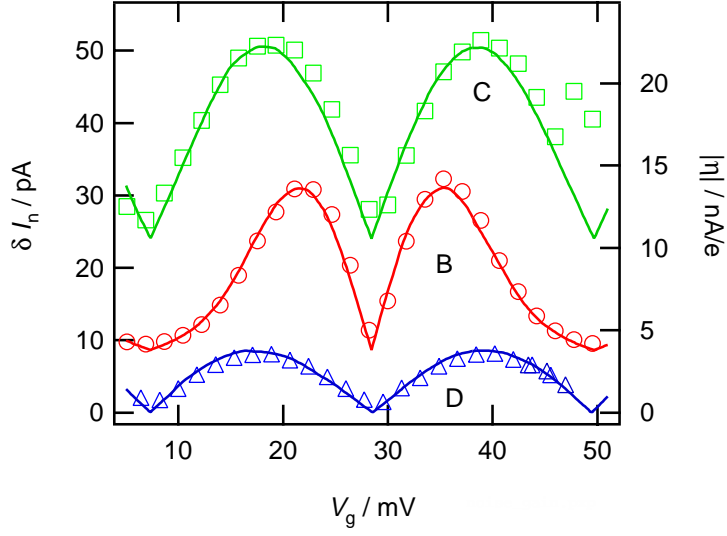


Figure 4.8: Integrated current noise, δI_N , and gain, η , vs. gate voltage for several bias voltages points (B, C, D). The curves have been offset vertically for clarity. Note the charge jump in trace C.

charge noise for the lowest and highest bias voltages, respectively, are currently not understood.

Next, a separation into input and output noise contributions using the simple model described by Eqs.(2.5) and (2.6) was tried. The resulting δQ_{in} for η_{max} is shown in Fig.(4.10). Since the input noise contribution δQ_{in} dominated, the error bars of the remaining noise, δI_{out} , became very large. The (1σ) error bars of output noise contribution, δI_{out} , was approximately five to ten times larger than the mean value. Only for two bias points out of the 130, (the highest bias voltage with lowest gain η), did δI_{out} have low error bars. δI_{out} was 1.6 ± 0.3 pA for both these bias points. An estimate for the resistance fluctuation was then determined. First however, the second order gain effects must be estimated by calculating $\alpha(f)$ (see Eq.(2.7)). From this calculation, it was found that $\alpha(f) \leq 10^{-4}$. The strength of second order noise is approximately α multiplied by the maximum charge noise. However, the dynamic noise range was about 100. As a consequence, the second order noise was masked by preamplifier noise. Thus, second order effects were negligible. Finally, by assuming that $\delta Q_{q,n} = \delta Q_{in}$ (*i.e.* $S_{Q_g} = S_{in}$), the resistance fluctuations were calculated from Eq.(2.11) yielding a resistance fluctuation $\delta R_n \approx 1.5 \pm 0.3 \Omega_{RMS}$. The correlation term was not dominant, and δR_n changed about 10% for $-1 \leq K \leq 1$ (included in the figure above). Repeating the above analysis for the *Nb* SET, a resistance fluctuation of $\delta R_n \approx 27.5 \pm 3.0 \Omega_{RMS}$ was found. Second order gain effects were masked by preamplifier noise.

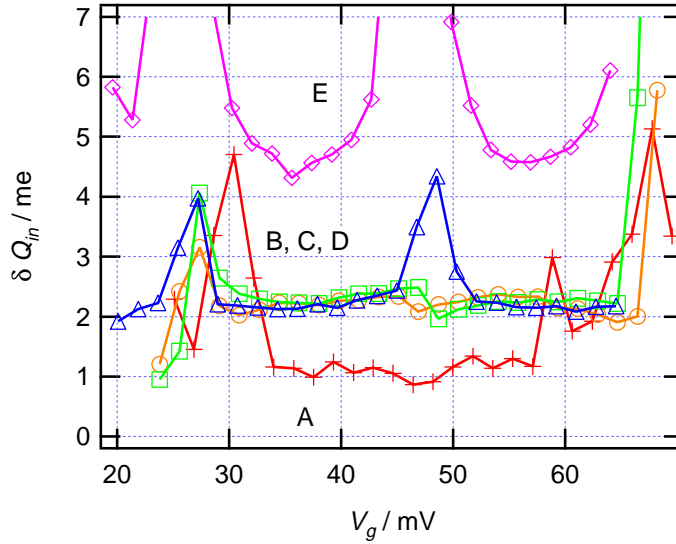


Figure 4.9: Input referred, integrated noise for the five voltage bias points. The lowest curve (+) is for the lowest bias point (A), while the uppermost curve (\diamond) is for the voltage highest bias point (E). The three curves in between (\circ \square \triangle) are for intermediate bias voltage points (B, C, D).

4.3 Niobium SET Noise Characteristics

In appended paper 3, the bias and temperature dependence of the low frequency noise of a *Nb* SET was investigated. 210 bias points in the normal state was noise characterized. The SET had an island capacitance of $C_\Sigma \approx 0.49$ fF and an asymptotic resistance of $R_N \approx 170$ k Ω . The gate capacitance was low, $C_g \approx 0.31$ aF, and the maximum gain was $\eta \approx 1.7$ nA/e. The gain was determined from the IQ_g characteristics. Due to the sparseness of gate bias points, the gain error bars became larger than for the *Al* SET.

Instead of integrating the noise in a band, the noise spectra were fitted to a $1/f$ function. Then, the 10 Hz output noise ($S_{I,fit}(f = 10 \text{ Hz})$) was compared to the gain. It was found that the noise followed the gain as in the *Al* SET (see Sec.(4.2.5) above). Furthermore, the input noise magnitude increased with the bias voltage in a more pronounced way than for the *Al* SET. At high temperatures, this dependence disappeared. The interpretation of these two facts were that either heating or the bias current activated TLFs either in the vicinity of the island, or in the junction dielectric.

The noise in appended paper 3 was analyzed in a slightly different manner than in appended paper 2. Nevertheless, resistance fluctuations were found and had essentially the same dependence on bias voltage.

4.4 Discussion and Future work

The method of mapping noise and gain provides insight in the origin of the noise sources. A separation into input and output acting noise sources has phys-

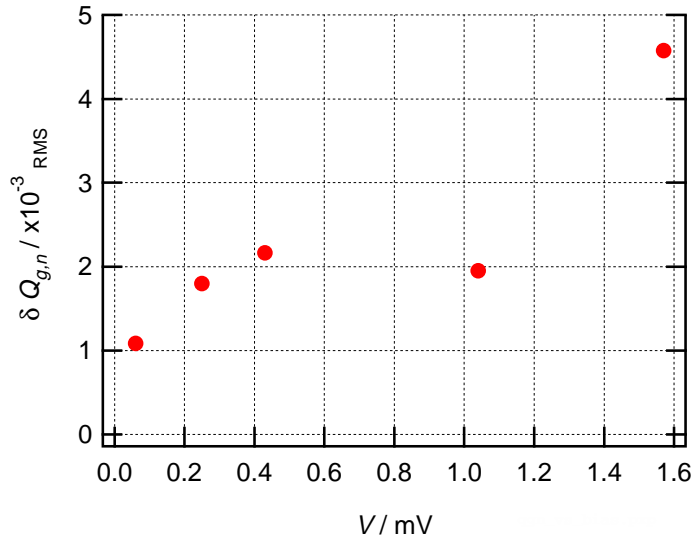


Figure 4.10: Integrated charge noise for the five voltage bias points.

ical meaning. Different noise processes can be separated into input and output sources. This is very clear from the data of the low ohmic *Al* SET, where the dominant noise source is acting as a charge fluctuator, but a very small contribution was found which possibly could be due to resistance fluctuations. In the *Nb* SET, the charge noise was dependent on both bias voltage and temperature. A resistance fluctuation contribution was found and was larger than in the *Al* SET.

To be able to separate the sources better, it is very important to measure the noise in bias points with zero gain. Then, the charge noise sources are completely shut off from the measurement. However, if the zero gain point is missed by a small amount and the SET has large charge noise, second order gain effects will show up and distort the spectrum. This will make the separation very difficult. In such cases, the best way to proceed is probably to step the gate bias in very small amounts around the $\eta = 0$ bias point. The spectrum can then be studied as it is distorted by different amounts and the gain minimum can be found.

The greatest problem, by far, during the measurements was that of not being able to directly measure the gain. Instead, gain data from the SET and SPICE simulations were used to predict the gain. This led to inaccuracies and limited the bandwidth. Considerable effort was put into the gain determination, and it was very time consuming. The consequence of the inaccuracy is simply that the charge noise is not very well determined for high frequencies. The reason for the inability to measure gain is crosstalk. If the crosstalk is diminished, the effort in mapping noise and gain will be dramatically reduced.

Currently, a new high frequency cryostat is installed at Chalmers, with several coaxial cables leading directly to the sample holder. This will reduce crosstalk by several orders of magnitude, and will enable high accuracy measurements of the gain. The coaxial cable also presents a much lower capacitance than the cables in the present setup. This will shift the rising noise term up in

frequency by one order of magnitude and may enable direct observation of the shot noise. (Using the shot noise detection formula, Eq.(3.13) with $I = 1$ nA and preamplifier parameters gives, an upper frequency of $f = 9.5$ kHz. This may be possible with SETs with low $1/f$ noise.) Moreover, a coaxial line will present a more ideal line capacitance, making the preamplifier easier to compensate. Thus, it is the author's hope that noise mapping will be a much simpler task using the new setup in the future.

From a device point of view, the superconducting SET is superior to the normal SET. If the SET is voltage biased, the gap induces a large gain increase which amplifies the signal and noise more, and the output noise is larger. This allows higher input noise of the following preamplifier. Also, a gain increase should be possible by decreasing the asymptotic resistance of the SET. A gain maximum would probably be found for lower impedances than in the normal case. The output impedance, r_o , of the SET should be made so low that the voltage noise of the preamplifier almost dominates the noise spectrum (see Eq.(3.12)). Low impedance SETs are also needed for RF SETs [16]. Thus, the development of superconducting SETs is very important. If niobium devices with high gap can be fabricated, one can expect a large increase not only in operating temperature, but also in gain. Activity is under way at Chalmers, PTB and NEC to produce niobium SETs. To conclude, the future of the SET looks very good, since increases in both noise performance, bandwidth and temperature of operation are expected.

Chapter 5

Conclusions

To conclude, the low frequency noise of two Single Electron Transistors was studied. Both *Al* and *Nb* based transistors were measured. A phenomenological model for charge and resistance fluctuations was derived, which allows separation of these contributions. By mapping noise and gain for a large number of bias points, the model was used to separate resistance and charge fluctuations. The *Al* transistor was dominated by a large charge noise source, and resistance fluctuations were only found at the highest bias point where the gain was low. In the frequency band 51 - 99 Hz, the resistance fluctuations were estimated to $\delta R_n \approx 1.5 \pm 0.3 \Omega_{RMS}$. The *Nb* transistor was, for low bias voltages dominated by a somewhat weaker charge noise source than the *Al* transistor. At high bias voltages the charge noise increased much, and the resistance fluctuations were $\delta R_n \approx 27.5 \pm 3.0 \Omega_{RMS}$. The bias and temperature dependence of the low frequency noise in the *Nb* transistor may be an effect of either heat or bias current activation of two level fluctuators located in vicinity of the island or in the junction dielectric. From the spectra, the highest sensitivity (defined as the noise level) were $q_n \approx 2 \cdot 10^{-5} \text{ e}/\sqrt{\text{Hz}}$ at $f = 4.5 \text{ kHz}$ for both transistors, which is the lowest achieved together with the RF-SET.

In order to measure noise more accurately, a low noise, current sensitive preamplifier was built. The preamp has two advantages over the voltage preamp. First, the bandwidth is larger and second, the bandwidth is insensitive to variations in the source impedance, r_o . This is in contrast to the voltage preamplifier, where the bandwidth is inversely proportional to r_o . The current preamp removed the need for bandwidth correction below 600 Hz.

Chapter 6

Acknowledgements

I would like to thank my supervisor Per Delsing for giving me the opportunity to work in his group. We have always had very stimulating discussions on physics and electronics.

Tord Claeson deserves many thanks. First for starting up the Swedish Nanometer Laboratory, without which it would not have been possible to fabricate the SETs. Second for reading my manuscripts, both for the papers and for the thesis.

Torsten Henning must be given credit for motivating me to use high quality software which has saved me enormous amounts of time. Also, his help with TeX is invaluable.

Alexander Korotkov for interesting discussions on the aspects of low frequency noise in the SET.

Dima Golubev for guiding an experimentalist through the various aspects on noise and SET theory.

Bibliography

- [1] Robert A. Millikan. *Phys. Rev.*, 2:109, 1913.
- [2] Paul S. Epstein. Robert Andrew Millikan as physicist and teacher. *Reviews of Modern Physics*, 20(1):10–25, January 1948.
- [3] K. K. Likharev. Single-electron transistors: Electrostatic analogs of the dc SQUIDS. *IEEE Trans. Magnetics*, MAG-23(2):1142–1145, March 1987.
- [4] T. A. Fulton and G. J. Dolan. Observation of single-electron charging effects in small tunnel junctions. *Phys. Rev. Lett.*, 59(1):109–112, July 1987.
- [5] L. J. Geerligs, V. F. Anderegg, P. A. M. Holweg, J. E. Mooij, H. Pothier, D. Esteve, C. Urbina, and M. H. Devoret. Frequency-locked turnstile device for single electrons. *Phys. Rev. Lett.*, 64(22):2691–2694, May 1990.
- [6] P. Delsing. One-dimensional arrays of small tunnel junctions. In Hermann Grabert and Michel H. Devoret, editors, *Single Charge Tunneling. Coulomb Blockade Phenomena in Nanostructures*, volume 294 of *NATO ASI Series*, chapter 7, pages 249–274. Plenum Press, New York, 1992. ISBN 0-306-44229-9.
- [7] H. Pothier, P. Lafarge, C. Urbina, D. Esteve, and M. H. Devoret. Single-electron pump based on charging effects. *Europhys. Lett.*, 17(3):249–254, 1992.
- [8] John M. Martinis, M. Nahum, and Hans Dalsgaard Jensen. Metrological accuracy of the electron pump. *Phys. Rev. Lett.*, 72(6):904–907, February 1994.
- [9] Konstantin K. Likharev and Tord Claeson. Single electronics. *Scientific American*, 266(6):80–85, June 1992.
- [10] D. V. Averin and K. K. Likharev. Single electronics: A correlated transfer of single electrons and Cooper pairs in systems of small tunnel junctions. In B. L. Altshuler, P. A. Lee, and R. A. Webb, editors, *Mesoscopic Phenomena in Solids*, volume 30 of *Modern Problems in Condensed Matter Sciences*, chapter 6, pages 173–272. North-Holland, Amsterdam, 1991.
- [11] Yasunobu Nakamura, ChiiDong Chen, and Jaw-Shen Tsai. 100-K operation of Al-based single-electron transistors. *Jpn. J. Appl. Phys.*, 35:L1465–L1467, November 1996.

- [12] D. V. Averin and Yu. V. Nazarov. Macroscopic quantum tunneling of charge and co-tunneling. In Hermann Grabert and Michel H. Devoret, editors, *Single Charge Tunneling. Coulomb Blockade Phenomena in Nanostructures*, volume 294 of *NATO ASI Series*, chapter 6, pages 217–247. Plenum Press, New York, 1992. ISBN 0-306-44229-9.
- [13] D. S. Golubev and A. D. Zaikin. Strong electron tunneling through a small metallic grain. *JETP-Letters*, 63(12):1007–1012, June 1996.
- [14] P. Joyez, V. Bouchiat, D. Esteve, C. Urbina, and M.H. Devoret. Strong tunneling in the single-electron transistor. *Phys. Rev. Lett.*, 79(7):1349–1352, August 1997.
- [15] D. Golubev. private communication, 1998.
- [16] R. J. Schoelkopf, P. Wahlgren, A. A. Kozhevnikov, P. Delsing, and D. E. Prober. The radio-frequency single-electron transistor (RF-SET): A fast and ultrasensitive electrometer. *Science*, 280:1238–1242, May 1998.
- [17] J. M. Hergenrother, M. T. Tuominen, T. S. Tighe, and M. Tinkham. Fabrication and characterization of single-electron tunneling transistors in the superconducting state. *IEEE Trans. Appl. Supercond.*, 3(1):1980–1982, March 1993.
- [18] D. Song, A. Amar, C. J. Lobb, and F. C. Wellstood. Advantages of superconducting Coulomb-blockade electrometers. *IEEE Trans. Appl. Supercond.*, 5(2):3085–3089, June 1995.
- [19] Alexander N. Korotkov. Charge sensitivity of superconducting single-electron transistor. *Appl. Phys. Lett.*, 69(17):2593–2595, October 1996.
- [20] A. N. Korotkov, D. V. Averin, K. K. Likharev, and S. A. Vasenko. Single-Electron Transistors as Ultrasensitive Electrometers. In H. Koch and H. Lübbig, editors, *Single-Electron Tunneling and Mesoscopic Devices*, volume 31 of *Springer Series in Electronics and Photonics*, pages 45–59. Springer, Berlin, 1992.
- [21] L. S. Kuzmin, P. Delsing, T. Claeson, and K. K. Likharev. Single-electron charging effects in one-dimensional arrays of ultrasmall tunnel junctions. *Phys. Rev. Lett.*, 62(21):2539–2542, May 1989.
- [22] L. J. Geerligs, V. F. Anderegg, and J. E. Mooij. Tunneling time and offset charging in small tunnel junctions. *Physica B*, 165/166:973–974, 1990.
- [23] G. Zimmerli, T. M. Eiles, R. L. Kautz, and John M. Martinis. Noise in the Coulomb blockade electrometer. *Appl. Phys. Lett.*, 61(2):237–239, July 1992.
- [24] A. B. Zorin, F.-J. Ahlers, J. Niemeyer, T. Weimann, H. Wolf, V. A. Krupenin, and S. V. Lotkhov. Background charge noise in metallic single-electron tunneling devices. *Phys. Rev. B*, 53(20):13682–13687, May 1996.
- [25] Vincent Bouchiat. *Quantum fluctuations of the charge in single electron and single Cooper pair devices*. PhD thesis.

- [26] A. N. Tavkhelidze and J. Mygind. Low-frequency noise in single electron tunneling transistor. *J. Appl. Phys.*, 83(1):310–317, January 1998.
- [27] A. B. Zorin. The thermocoax cable as the microwave frequency filter for single electron circuits. *Rev. Sci. Instrum.*, 66(8):4296–4300, August 1995.
- [28] D. Vion, P. F. Orfina, P. Joyez, D. Esteve, and M. H. Devoret. *J. Appl. Phys.*, 77:2519, 1995.
- [29] A.N. Korotkov. private communication, 1998.
- [30] W. Schottky. Über spontane Stromschwankungen in verschiedenen Elektrizitätsleitern. *Annalen der Physik, Vierte Folge*, 57 (362 der ganzen Reihe):541–567, 1918.
- [31] H. Birk, M. J. M. de Jong, and C. Schönenberger. Shot-noise suppression in the single-electron tunneling regime. *Phys. Rev. Lett.*, 75(8):1610–1613, August 1995.
- [32] Paul Horowitz and Winfield Hill. *The Art of Electronics*. Cambridge University Press, Cambridge, 2nd edition, 1989. ISBN = 0-521-37095-7.
- [33] E. H. Visscher, S. M. Verbrugh, J. Lindeman, P. Hadley, and J. E. Mooij. Fabrication of multilayer single-electron tunneling devices. *Appl. Phys. Lett.*, 66(3):305–307, January 1995.
- [34] S. M. Verbrugh, M. L. Benhamadi, E. H. Visscher, and J. E. Mooij. Optimization of island size in single electron tunneling devices: Experiment and theory. *J. Appl. Phys.*, 78(4):2830–2836, August 1995.
- [35] B. Starmark, P. Delsing, D. B. Haviland, and T. Claeson. Noise measurements of single electron transistors using a transimpedance amplifier. In H. Koch and S. Knappe, editors, *ISEC'97. 6th International Superconductive Electronics Conference. Extended Abstracts*, volume 2, pages 391–393, Berlin, June 1997. Physikalisch-Technische Bundesanstalt. ISBN 3-9805741-0-5.
- [36] A. B. Zorin, Yu. A. Pashkin, V. A. Krupenin, and H. Scherer. Single Cooper pair electrometer based on Bloch transistor in a high impedance environment. In H. Koch and S. Knappe, editors, *ISEC'97. 6th International Superconductive Electronics Conference. Extended Abstracts*, volume 2, pages 394–396, Berlin, June 1997. Physikalisch-Technische Bundesanstalt. ISBN 3-9805741-0-5.
- [37] V. A. Krupenin, D. E. Presnov, M. N. Sarateev, H. Scherer, A. B. Zorin, and J. Niemeyer. Noise in Al single electron transistors of stacked design. *cond-mat/9804197*, April 1998.
- [38] G. Zimmerli, R. L. Kautz, and John M. Martinis. Voltage gain in the single-electron transistor. *Appl. Phys. Lett.*, 61(21):2616–2618, November 1992.
- [39] Aldert van der Ziel. *Noise in solid state devices and circuits*. Wiley, New York, 1986. ISBN = 0-471-83234-0.

- [40] Stefan Machlup. Noise in semiconductors: Spectrum of a two-parameter random signal. *J. Appl. Phys.*, 25(3):341–343, March 1954.
- [41] C. T. Rogers, R. A. Buhrman, W. J. Gallagher, S. I. Raider, A. W. Kleinsasser, and R. L. Sandstrom. Electron trap states and low frequency noise in tunnel junctions. *IEEE Trans. Mag.*, MAG-23(2):1658–1661, March 1987.
- [42] Neil M. Zimmerman, Jonathan L. Cobb, and Alan F. Clark. Modulation of the charge of a single-electron transistor by distant defects. *Phys. Rev. B*, 56(12):7675–7678, September 1997.
- [43] S. Bengtsson. Department of Solid State Electronics, Chalmers, Göteborg, private communication, 1998.
- [44] Jürgen Niemeyer. Eine einfache Methode zur Herstellung kleinster Josephson-Kontakte. *PTB-Mitt.*, 84(4):251–253, 1974.
- [45] G. J. Dolan. Offset masks for lift-off photoprocessing. *Appl. Phys. Lett.*, 31(5):337–339, September 1977.
- [46] Peter Wahlgren. Local and global rules for the Coulomb blockade in ultra-small tunnel junctions. Licentiate thesis, Department of Physics, Chalmers University of Technology and Göteborg University, Göteborg, 1995.
- [47] J. Pettersson, P. Wahlgren, P. Delsing, D. B. Haviland, T. Claeson, N. Rorsman, and H. Zirath. Extending the high-frequency limit of a single-electron transistor by on-chip impedance transformation. *Phys. Rev. B*, 53(20):R13272–R13274, May 1996.
- [48] Walter G. Jung. *Audio IC Op-Amp Applications*. Howard W. Sams & Co., Indianapolis, 3rd edition, 1987. ISBN = 0-672-22452-6.
- [49] Walter G. Jung. *IC Op-Amp Cookbook*. Howard W. Sams & Co., Indianapolis, 3rd edition, 1986. ISBN = 0-672-22453-4.
- [50] Analog Devices. AD743 data sheet: Ultralow noise BIFET opamp. <http://www.analog.com/>.
- [51] Jerald Graeme. *Photodiode amplifiers : op amp solutions*. McGraw-Hill, New York, 1996. ISBN = 0-07-024247-X.
- [52] L. W. Nagel and D. O. Pederson. Simulation program with integrated circuit emphasis (SPICE). ERL-M382, University CA, Berkely, 1973.
- [53] Don Lancaster. *Active Filter Cookbook*. Newnes, Oxford, 2nd edition, 1995. ISBN = 0 7506 2986 X.
- [54] P. Wahlgren, P. Delsing, and D. B. Haviland. Crossover from global to local rule for the Coulomb blockade in small tunnel junctions. *Phys. Rev. B*, 52(4):R2293–R2296, July 1995.
- [55] D. V. Averin, A. N. Korotkov, A. J. Manninen, and J. P. Pekola. Resonant tunneling through a macroscopic charge state in a superconducting single electron transistor. *Phys. Rev. Lett.*, 78(25):4821–4824, June 1997.

Appendix A

List of Symbols

Symbol	meaning
$\alpha(f)$	SET Second Order Gain, see Eq.(2.7)
α_t	SET Normalized Asymptotic Resistance
δI_n	SET Integrated Current Noise, see Eq.(4.1)
δI_{out}	SET Integrated Output Source Noise, see Eq.(4.3)
δQ_{in}	SET Integrated Input Source Noise, see Eq.(4.2)
$\delta Q_{q,n}$	SET Integrated Charge Noise, see Eq.(4.4)
δR_n	SET Integrated Resistance Noise, see Eq.(4.5)
Δ	Superconducting Gap Energy
ΔI	SET Current Modulation, see Eq.(1.5)
ΔV	SET Voltage Modulation
η	SET Charge to Current Gain, see Eq.(1.10)
κ_i	SET Resistance to Current Gain, see Eq.(1.14)
ω_0	Op Amp -3dB Frequency of $A_{ol}(\omega)$
A_o	Op Amp DC Open Loop gain
$A_{ol}(\omega)$	Op Amp AC Open Loop gain, see Eq.(3.5)
B	SET External Magnetic Field
C	Capacitance
C_0	Island Self Capacitance
C_Σ	Total SET Capacitance, see Eq.(1.1)
C_f	Preamplifier Feedback Capacitance, see Fig.(3.4)
C_i	SET Tunnel Junction Capacitance, $i =$ junction number
C_g	Gate Capacitance
C_{tot}	Preamplifier Total Load Capacitance, see Fig.(3.4)
E_C	SET Island Charging Energy, see Eq.(1.2)
E_J	Josephson Coupling Energy
$e_{n,op}$	Op Amp Input Equivalent Voltage Noise, see Fig.(3.7)
f_g	Preamplifier Bandwidth, see Eqs.(3.8) and (3.9)
G	Preamplifier DC Gain, see Eq.(3.1)
$G(\omega)$	Preamplifier AC Gain, see Eq.(3.6)
GBW	Op Amp Gain Bandwidth Product
g_m	SET Transconductance, see Eq.(1.11)
I	SET Bias Current
I_{b-}	Op Amp Bias Current, Inverting Input, see Eq.(3.3) and Fig.(3.3)
$i_{n,op}$	Op Amp Input Equivalent Current Noise, see Fig.(3.7)
i_{n,R_f}	Feedback Resistance Johnson Noise Current, see Fig.(3.7)
i_{in}	Preamplifier Total Input Referred Noise Current, see Eq.(3.12)
K	SET Total Charge/Resistance Correlation Coefficient
$k_B T$	Thermal Energy

K_i	SET Charge/Resistance Correlation Coefficient, $i =$ junction number
L_{eq}	Preamplifier Input Equivalent Inductance
Q_g	SET Gate Charge
q_n	SET Charge Noise Density
R_f	Preamplifier Feedback Resistance, see Fig.(3.2)
R_i	SET Tunnel Junction Resistance, $i =$ junction number
R_{in}	Preamplifier Input Resistance, see Eq.(3.2)
R_N	SET Asymptotic Resistance, see Eq.(1.3)
$R_{N,opt}$	SET Optimum Asymptotic Resistance, see Eq.(1.6)
r_o	SET Output or Dynamical Resistance, see Eq.(1.13)
R_Q	Quantum of Resistance, see Eq.(1.4)
$S_I(\omega)$	SET Current Noise Spectrum
$S_{I,Q,R}(\omega)$	SET Charge and Resistance Fluctuation Output Spectrum, see Eq.(2.8)
$S_{in}(\omega)$	SET Input Noise Source Spectrum, see Eq.(2.5)
$S_{out}(\omega)$	SET Output Noise Source Spectrum, see Eq.(2.6)
$S_R(\omega)$	SET Total Resistance Noise Spectrum, see Eq.(2.9)
$S_{R_i}(\omega)$	SET Resistance Noise Spectrum, $i =$ junction number, see Eq.(2.8)
T	Temperature
V	SET Bias Voltage
V_g	SET Gate Voltage
V_{os}	Op Amp Offset Voltage, see Eq.(3.3) and Fig.(3.3)
V_T	SET Threshold Voltage
$Z_{in}(\omega)$	Preamplifier AC Input Impedance, see Eq.(3.7)
$Z_T(\omega)$	Preamplifier Total AC Transfer Function, see Eq.(3.10)

Appendix B

Appended Paper 1

Noise Measurements of Single Electron Transistors using a Transimpedance Amplifier

B. Starmark, P. Delsing, D.B. Haviland and T. Claeson

Department of Microelectronics and Nanoscience, Chalmers University of Technology and Göteborg University
S-412 96 Göteborg, Sweden

Abstract — We have measured a Single Electron Transistor (SET) using a transimpedance amplifier which increases the bandwidth of the SET by two orders of magnitude compared to the conventional voltage sensitive amplifier. Using this amplifier to measure the properties of the SET we find a bandwidth of 6.2 kHz and measure the SET noise density up to 1 kHz. The noise is $\delta Q_n \approx 3.9 \cdot 10^{-5} e/\sqrt{\text{Hz}}$ at 300 Hz.

I. INTRODUCTION

The Single Electron Transistor (SET) [1], [2] is the most sensitive electrometer to date. It consists of a small metallic island to which two electrodes are coupled via tunnel junctions. The island is very sensitive to any external electric field which can modulate the current transport properties of the system. In order to operate correctly the tunnel resistance of the junction must be larger than $R_Q = h/(4e^2) \approx 6.45 \text{ k}\Omega$. Furthermore the capacitive coupling C_Σ of the island to the ambient must be so small that the charging energy obeys $E_C = e^2/(2C_\Sigma) \gg k_b T$.

With today's lithographic techniques, metallic SET devices must normally operate at $T = 1 \text{ K}$ or below, which means that experiments must be carried out in a cryostat. However, recent improvements in the lithographic techniques have made SET devices operating at 100 K possible [3]. Usually, SET-based electrometers have been biased via a resistor and the voltage drop has been measured. The measurement leads from the cooled SET to the room temperature electronics form a capacitance C_l which shunts the voltmeter at high frequencies, limiting system bandwidth. The bandwidth is given by $(2\pi R_o C_l)^{-1}$ where R_o is the total resistance at the output yielding typical bandwidths on the order of 100 Hz. SET/HEMT hybrids can reach substantially higher bandwidths [4], [5] but so far the noise above 100 Hz in these systems has been dominated by the HEMT.

Measurements of the charge noise density as a function of frequency for normal conducting SETs have been reported by several groups [6], [7], [8] with noise densities as low as $7 \cdot 10^{-5} e/\sqrt{\text{Hz}}$ at 10 Hz [6]. Also, noise measurements on a Bloch transistor have been reported [9]. Most measurements have been carried out at frequencies up to 10 Hz and no one has, to our knowledge, measured the noise spectrum of a SET above 200 Hz due to the low bandwidth.

The samples were fabricated in the Swedish Nanometer Laboratory, Göteborg. We were sponsored by the Swedish NFR, SSF and thru the European Union ESPRIT programme MEL ARI, project 22953 CHARGE.

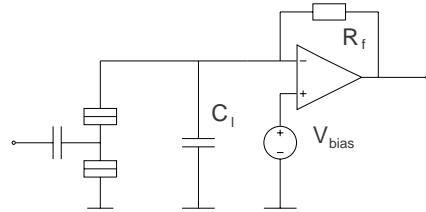


Fig. 1: A simplified scheme of the SET and the transimpedance amplifier. R_f is the feedback resistor, C_l the line capacitance and V_{bias} is the external bias voltage source. In the experiment we used a symmetric version of the amplifier.

Here we show that by measuring the current through the SET, rather than the voltage across it, the system bandwidth is greatly increased. In principle, we connect an Ampere meter across the SET electrodes which shunts the capacitance. This is in contrast with the conventional voltage measurement system where the capacitance shunts the voltmeter. The technique we use is well known in electronics and is used for measuring high impedance sources such as photodiodes [10]. In practice, our Ampere meter is an op amp connected as current/voltage converter, which we will refer to as a transimpedance amplifier. We have designed and implemented such a transimpedance amplifier and here we report on measurements of the frequency response and the noise density of a SET transistor.

II. CIRCUIT AND MEASUREMENT TECHNIQUES

A simplified scheme of the SET and the transimpedance amplifier is shown in Fig. 1. The inverting input works as a low impedance current input. The op amp output is fed back via the resistor R_f . The feedback loop forces the inverting input of the op amp to the same potential as the non-inverting input, thereby voltage biasing the SET to a voltage of V_{bias} . A current passed into the input is converted to a voltage by R_f which sets the gain of the amplifier. The input impedance R_{in} of the circuit is given by $R_f/A_{vol}(f)$ where $A_{vol}(f)$ is the frequency dependent open loop voltage gain of the op amp. Note that R_{in} is a function of frequency. To achieve dc accuracy, the signal source must have a much higher impedance than R_{in} . This is a natural demand for SET devices since the transistor resistance must obey $R_t > R_Q$ for proper SET

operation and by setting $R_{in} \ll R_Q$, good dc accuracy is automatically achieved.

Since the measured signal from the SET is a current, one should maximize the $\Delta V/R_t$ ratio of the SET to maximize the signal, which differs from the voltage signal case where ΔV alone should be maximized. The maximum modulation can be calculated from a simple model derived by Golubev [11] which yields an optimal junction resistance of $\sqrt{2}R_Q \approx 9.1 \text{ k}\Omega$.

The most important advantage of the transimpedance amplifier is the increased bandwidth when using it with high impedance sources. The low R_{in} shunts any capacitive load at the input of the amplifier. A simple model for the amplifier system yields a bandwidth of

$$f_c = \sqrt{\frac{\text{GBP}}{2\pi R_f C_l}} \quad (1)$$

where GBP is the gain bandwidth product of the op amp. Thus, the bandwidth is set by components situated at room temperature, yielding a very flexible system. Furthermore, the bandwidth scales with the inverse square root of C_l .

The amplifier is very sensitive to a capacitive load on the inverting input, which can lead to instability. By lowering the GBP one regains stability at the expense of bandwidth. This is done by connecting a capacitor in parallel with R_f . Another drawback of the capacitance C_l is that it introduces an extra noise term which rises linearly with frequency and is given by

$$i_n = 2\pi e_n f C_l \quad (2)$$

where e_n is the voltage noise of the op amp. This severely lowers the signal to noise ratio at high frequencies.

The SET was fabricated of aluminum, using e-beam lithography and the standard angle evaporation technique.

Measurements were made in a dilution refrigerator at a temperature of 20 mK. To quench superconductivity a magnetic field of 2 T was applied. The SET transistor was connected to the room temperature electronics through dc lines with $C_l \approx 1 \text{ nF}$. Due to large crosstalk of the gate signal to the drain line it was difficult to separate the real output from parasitic signal when the input was a sinusoidal signal. Instead we used the same technique as in [4] where a ramp was applied to the gate, tracing out several modulation periods which reduced the crosstalk to discrete spikes at the ramp high to low switch. The spikes were removed at the output of the amplifier by gating the signal. The modulation was then used as the signal. By changing the ramp frequency the modulation was made faster.

III. RESULTS

From the current-voltage characteristics a total transistor resistance of $R_t = 415 \text{ k}\Omega$ was deduced. The total capacitance of the SET was $C_\Sigma = 149 \text{ aF}$ and was found from the

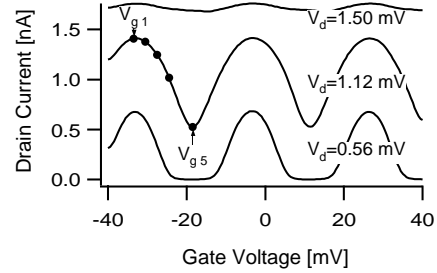


Fig. 2: Current modulation versus gate voltage for different fixed drain voltages. The dot markers show the five gate voltage points V_{g1} to V_{g5} .

offset voltage using a technique described by Wahlgren et al. [12]. The current modulation for three different voltage biases is shown in Fig. 2. The maximum modulation was $I = 0.90 \text{ nA}$ peak to peak for $V_d = 1.12 \text{ mV}$. The periodicity of the gate voltage was $\Delta V_g = 30 \text{ mV}$, which corresponds to a gate capacitance of $C_g = 5.3 \text{ aF}$.

The frequency response was measured at the bias voltage with maximum modulation at $V_d = 1.12 \text{ mV}$ using both the transimpedance amplifier and for comparison a conventional resistor bias/voltage measurement amplifier. The feedback resistors were $820 \text{ k}\Omega$ in the former case and the bias resistors were $1 \text{ M}\Omega$ in the latter. The responses were normalized to their respective dc values, and are shown in Fig. 3. The superior bandwidth of the transimpedance amplifier is clearly seen. In this preliminary version of the amplifier, the GBP of the op amps had to be lowered by more than three orders of magnitude to retain stability. It should be possible to further increase bandwidth by a factor of five to ten by optimizing the room temperature electronics.

In Fig. 4 two spectra, taken at $V_g = V_{g4} = -24.5 \text{ mV}$ and $V_d = 1.12 \text{ mV}$ and $V_d = 0.56 \text{ mV}$, are shown to-

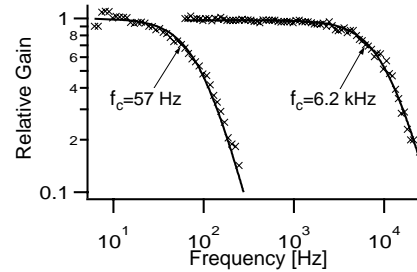


Fig. 3: Frequency response for the SET when measured with a voltage amplifier (left curve) and a transimpedance amplifier (to the right).

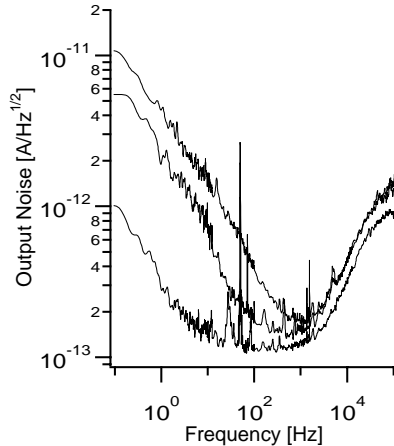


Fig. 4: Noise spectra for the system for $V_g = -24.5$ mV. The upper curve corresponds to $V_d = 1.12$ mV, the middle to $V_d = 0.56$ mV while the lower shows the preamplifier noise with no SET connected.

gether with the spectrum that was taken with the SET transistor removed to characterize the amplifier. There are two distinct areas seen in each spectrum: for low frequencies the SET $1/f$ noise dominates, and for high frequencies the noise is dominated by the f noise term due to the capacitive load C_i at the input of the amplifier (see eq. 2). The noise floor of the amplifier was $i_n \approx 0.2$ pA/ $\sqrt{\text{Hz}}$, which is the Johnson noise of the feedback resistors. The noise rises above this value for drain bias with maximum modulation, which gives the maximum gain of the SET. The maximum gain for our SET was found at $V_g = -23$ mV and $V_d = 1.12$ mV, where the gain was $dI/dQ_g = 3.2$ nA/e. The noise minimum at this bias point was $\delta Q_n \approx 3.9 \cdot 10^{-5} e/\sqrt{\text{Hz}}$ at a frequency of 300 Hz.

Noise was measured for 25 bias points in a five by five matrix for the gate and drain voltages respectively. The five gate points are marked in Fig. 2. Spot noise at 10 Hz for all 25 bias points is shown in table 1. Comparing table 1 with the data in Fig. 2, a correspondence between large gain and large noise can be seen.

IV. CONCLUSIONS

We have shown that by using a transimpedance amplifier the bandwidth of SET transistors can be increased more than two orders of magnitudes as compared to the conventional voltage amplifier technique. The bandwidth is increased from 57 Hz to 6.2 kHz in our particular setup. The new amplifier made it possible to measure noise up to 1 kHz. We found a minimum noise density of $\delta Q_n \approx 3.9 \cdot 10^{-5} e/\sqrt{\text{Hz}}$ at 300 Hz. Optimization of the

Table 1: Current spot noise density in pA/ $\sqrt{\text{Hz}}$ at 10 Hz for 25 bias points. The noise is referred to the output of the SET.

	V_{g1}	V_{g2}	V_{g3}	V_{g4}	V_{g5}
V_d [mV]	-33.5	-30.5	-27.5	-24.5	-18.5
0.56	0.15	0.15	0.15	0.7	0.6
1.12	1.8	1.2	1.8	1.6	0.3
1.50	0.35	0.28	0.92	1.1	0.21
1.87	0.26	0.31	0.40	0.22	0.19
2.4	0.26	0.31	0.62	0.7	0.33

room temperature electronics should further increase the bandwidth by a factor of five to ten.

V. ACKNOWLEDGEMENTS

We gratefully acknowledge J. Forsell, D. Golubev, J. Pettersson and A.B. Zorin and for stimulating discussions.

REFERENCES

- [1] K.K. Likharev, IEEE Transactions on Magnetics, Vol. Mag-23 (1987), 1142
- [2] T.A. Fulton and G.J. Dolan, Phys. Rev. Lett., Vol 59 (1987), 109
- [3] Y. Nakamura, C.D. Chen and J-S. Tsai, Jpn. J. Appl. Phys. Vol 35 (1996), L 1465
- [4] J. Pettersson, P. Wahlgren, P. Delsing, D.B. Haviland, T. Claeson, N. Rorsman and H. Zirath, Phys. Rev. B 53 (1996)
- [5] E.H. Visscher, J. Lindeman, S. M. Verbrugh, P. Hadley, J.E. Mooij and W. van der Vleuten, Appl. Phys. Lett. 68 (1996), 2014
- [6] E.H. Visscher, S. M. Verbrugh, J. Lindeman, P. Hadley and J.E. Mooij, Appl. Phys. Lett. 66 (1995), 305
- [7] A.B. Zorin, F.-J. Ahlers, J. Niemeyer, T. Weimann, H. Wolf, V.A. Krupenin and S.V. Lotkhov, Phys. Rev. B 53 (1996), 13682
- [8] G. Zimmerli, T.M. Eiles, R.L. Kautz and J.M. Martinis, Appl. Phys. Lett. 61 (1992), 237
- [9] A.B. Zorin, Y.A. Pashkin, V.A. Krupenin and H. Scherer, ISEC 97 - in this issue.
- [10] P. Horowitz and W. Hill, The Art of Electronics, Cambridge University Press, Cambridge, 1980, pages 597-598.
- [11] D. Golubev, private communication.
- [12] P. Wahlgren, P. Delsing and D.B. Haviland, Phys. Rev. B 52 (1995), R2293

Appendix C

Appended Paper 2

Gain Dependence of the Noise in the Single Electron Transistor

B. Starmark, Torsten Henning, T. Claeson and P. Delsing
Department of Microelectronics and Nanoscience, Göteborg University
and Chalmers University of Technology, S-412 96 Göteborg, Sweden

A. N. Korotkov
Nuclear Physics Institute, Moscow State University, 119899 GSP, Moscow, Russia

October 7, 1998

Abstract

An extensive investigation of low frequency noise in single electron transistors as a function of gain is presented. Comparing the output noise with gain for a large number of bias points, it is found that the noise is dominated by external charge noise. For low gains we find an additional noise contribution which is compared to a model including resistance fluctuations. We conclude that this excess noise is not only due to resistance fluctuations. For one sample, we find a low minimum charge noise of $q_n \approx 2 \cdot 10^{-5} e/\sqrt{\text{Hz}}$ at a frequency of 4.4 kHz.

1 Introduction

With the introduction of the Single Electron Transistor (SET) one decade ago, it became possible to directly measure changes in charge quantities below that of an electron [1, 2]. Based on the Coulomb blockade, the device has been shown to be the most sensitive electrometer existing today. The sensitivity of the SET is predicted to be limited by the shot noise [3] generated when electrons tunnel across the tunnel barriers [4]. Shot noise was observed in a two junction structure (without gate) [5]. In most experiments involving SETs, the noise for low frequencies has been dominated by the device itself, whereas external sources set the noise limit for frequencies above the kHz regime.

Several experimental studies of low frequency noise of various SET configurations have been performed [6]-[18]. Below 1 kHz, $1/f$ noise is observed in all SETs regardless of mode of operation [7]-[16]. The input equivalent charge noise at 10 Hz in all these experiments is of the order of 10^{-3} to $10^{-5} e/\sqrt{\text{Hz}}$, with $2.5 \cdot 10^{-5} e/\sqrt{\text{Hz}}$ recently reported as the lowest figure [17]. Deviations from an

$1/f$ spectrum are often observed, usually in combination with telegraph noise [7, 15]. The source of the latter is believed to be random excitations of a single charge trap. Theoretically, the random trapping process of a single trap shows a Debye-Lorentzian power spectrum [19] which is also observed experimentally [8, 12, 13]. It has been shown that an ensemble of traps produces a $1/f$ noise spectrum, see *e.g.* [22].

There are at least three possible locations of these fluctuators: the tunnel junction dielectric, the substrate on which the device is fabricated, and the oxide layer covering the device. The role of the substrate has been examined in at least two sets of experiments [12, 18]. Those experiments did not show a strong dependence of the noise on the substrate material. The barrier dielectric has been proposed as the location of charge traps [8, 9, 15, 17]. The role of the surface oxide of the island has not yet been investigated.

Several groups have found that the noise at the output of the SET varies with the gain of the SET and that the maximum noise is found at the bias point with maximum gain [8]-[11]. This indicates that the noise source acts at the input of the device, *i.e.* as an external fluctuating charge. However, a detailed comparison of the noise to the gain has not been done.

In this Letter, we report the low frequency current noise of one Al/Al₂O₃/Al/Al₂O₃/Al SET and one Nb/Al₂O₃/Al/Al₂O₃/Nb SET and make a detailed comparison with the gain. (Hereafter, we will refer to the two SETs as the Al SET and the Nb SET). For the Al SET, we find that the noise follows the gain in such a manner that the SET is dominated by input noise for almost all values of bias and gate voltage. For the Nb SET however, we find a contribution from other sources when analysing the noise in the points where the gain is low.

2 Experimental Techniques

The samples were fabricated on oxidised Si substrates using electron beam lithography and the standard double-angle evaporation technique [20].

The resistance of the Al SET directly after fabrication was $R_T = R_1 + R_2 \approx 0.8$ k Ω , which after a storage for six months, had increased to $R_T \approx 45$ k Ω . The Nb SET had a resistance of $R_T \approx 170$ k Ω .

We used a symmetric, current sensitive amplifier which voltage biased the SET [10]. To optimize the preamplifier noise performance low noise operational amplifiers with low $1/f$ noise were used. Furthermore, the bias (feedback) resistors were chosen to $R_F = 10$ M Ω to lower the amplifier noise floor at low frequencies.

The SETs were attached to the mixing chamber of a dilution refrigerator which was cooled to a temperature below 30 mK. All measurement leads were filtered with 0.5 m Thermocoax [21] followed by capacitors to ground. The total line capacitance was $C_l=1$ nF.

Evaluating the frequency performance, we found a gain bandwidth of the

SET setup of 7.5kHz while the noise bandwidth was about 300 Hz (without any SET connected). Both these figures were set by the line capacitance and the preamplifier [10].

The noise spectra were recorded by a HP 35665A Dynamic Signal Analyzer, which performs real-time FFT analysis of the input signal. The frequency range from 1 to 10^5 Hz was divided into four subranges to increase the resolution. The time to acquire all noise data for one bias point was 5 min.

3 Results and Discussion

Two samples were tested. The current-voltage IV characteristics for the Al SET are shown in Fig. 1a, both for the normal and the superconducting state. A total island capacitance of $C_\Sigma = 0.19$ fF was deduced from the IV -curves. The Nb SET had $C_\Sigma = 0.48$ fF. The output impedance, $r_o = (\partial I/\partial V)$, was calculated from the IV curves. In the superconducting state r_o was always above $20\text{k}\Omega$ while in the normal state, r_o was on the order of, or above R_T for both SETs. The gate coupling capacitances were $C_g \approx 4.8$ aF and $C_g \approx 0.3$ aF for the Al and the Nb SETs, respectively.

Due to its low resistance, the Al SET had a very high maximum gain of $\partial I/\partial Q_g = 12$ nA/e and $\partial I/\partial Q_g = 34$ nA/e in the normal and superconducting states, respectively. The Nb SET had $\partial I/\partial Q_g = 1.8$ nA/e and $\partial I/\partial Q_g = 3.8$ nA/e in the normal and superconducting states. The gain increase in the superconducting state is in accordance with earlier observations [14, 15].

Noise spectra for the normal and superconducting states of the Al SET are shown in Fig. 1b. Each spectrum has been referred to the input of the SET by dividing by the frequency dependent gain. The spectra N and S were measured at the bias points which gave maximum gain. For reference, a spectrum with no SET connected, R, is also shown and is divided by the same gain as in the normal state to obtain the input referred noise floor set by the amplifier. Minimum charge noises of $q_n \approx 2 \cdot 10^{-5} e/\sqrt{\text{Hz}}$ at a frequency of 4.4kHz was found both in the superconducting and normal states. The limit is set by the preamplifier and mechanical resonances within the cryostat. These numbers are, to our knowledge, the lowest values reported for any SET. The noise at 10 Hz was $9 \cdot 10^{-4} e/\sqrt{\text{Hz}}$ for both the superconducting and normal states. A cross-over from input dominated to output dominated noise can be seen as the frequency increases. Below 1 kHz, the input referred noise is almost the same in both normal and superconducting states, indicating that the noise source acts as an apparent charge noise, and thus is independent of gain. Above 5 kHz the noise is dominated by sources acting at the output of the SET. When referred to the input, this noise appears as a lower equivalent charge noise in the superconducting state as compared to the normal state, due to the higher gain in the superconducting state.

We now turn our attention to the noise below 1 kHz. To determine the origin

of the noise, we measured noise for 130 bias and gate voltages and compared it with the measured gain of the SET. All points were taken in the normal state at a temperature of $T \approx 30$ mK. The output current noise and the gain versus gate bias for the Al SET are shown in fig. 2a for three bias voltages. To reduce fluctuations, the noise was integrated in the band 51 to 99 Hz. By using the gate charge offset as the only fitting parameter, we were able to get an excellent fit of the noise to the gain. This result clearly shows that the noise source acts at the input of the SET. It is supposedly due to the motion of background charges somewhere in the vicinity of the SET-transistor. For the points of large gain we can deduce the spectral density of the charge fluctuations, $S_{Q_g}(f)$. The Nb SET also showed a gain dependent output noise, but with more spread in the data.

In bias points with low gain (high bias or $Q_g \approx ne/2$) it is possible to examine other noise contributions. For each V , we define the excess noise current as

$$I_{n,\text{exc}}^2(V) = \left(\int_{51 \text{ Hz}}^{99 \text{ Hz}} S_{I,\text{min}} df - \frac{G_{\text{min}}^2}{G_{\text{max}}^2} \int_{51 \text{ Hz}}^{99 \text{ Hz}} S_{I,\text{max}} df \right) / \left(1 - \frac{G_{\text{min}}^2}{G_{\text{max}}^2} \right) \quad (1)$$

where $S_{I,\text{min}}$, G_{min} and $S_{I,\text{max}}$, G_{max} are the measured current power spectra and gains for each V at minimum and maximum gain respectively. This quantity is zero when the gain dependent noise is the only contribution.

The Al SET showed excess noise only at the highest bias point, 2.6 ± 0.97 pA²/Hz, whereas the Nb SET showed excess noise at several bias points. To gain more knowledge about the noise contributions we next discuss the different components of the measured noise.

Except for charge noise sources somewhere in the vicinity of the transistor, current noise can also be induced by fluctuations in the tunnel barrier resistance. As we will see, these two contributions can generally not be separated. There are also contributions from shot noise and amplifier noise. In our case, the amplifier noise is dominated by the thermal noise of the two feedback resistors and the noise generated by the input equivalent voltage noise, e_n , of the amplifier. For low temperatures, the shot noise is given by $S_I = aeI$, where $1 \leq a \leq 2$, with $a = 2$ for strongly correlated tunneling and $a = 1$ for uncorrelated tunneling [4]. The total measured current noise in the system can be modelled by

$$S_{I_m}(f) = 2k_B \frac{T_F}{R_F} + \frac{e_n^2(f)}{2r_0^2} + aeI + S_{I_{Q,R}}(f) \quad (2)$$

where T_F is the temperature of the feedback resistors and $S_{I_{Q,R}}(f)$ is the combined spectral density due to charge and resistance fluctuations. The first two terms represent amplifier noise and are frequency independent in the range of interest (51-99 Hz). The third term is the shot noise of the SET which also is independent of frequency. These terms are of order $(30 \text{ fA})^2/\text{Hz}$ for the worst

case with lowest r_o and high I . Thus, the sum of these three terms varies only slightly between $(30 \text{ fA})^2/\text{Hz}$ and $(50 \text{ fA})^2/\text{Hz}$ for all bias points. To evaluate the last term let us start with a model in which the only fluctuating parameter is the background charge Q_g . Assuming small variations we can write

$$\delta I = \frac{\partial I}{\partial Q_g} \delta Q_g + \frac{1}{2} \frac{\partial^2 I}{\partial Q_g^2} (\delta Q_g)^2 + \dots \quad (3)$$

If only the first (linear) term is taken into account, then obviously $S_{I_Q}(f) = (\partial I / \partial Q_g)^2 S_{Q_g}(f)$ where S_{Q_g} and S_{I_Q} are the background charge spectral density and the charge induced current spectral density. As seen in fig. 2a we are close to this situation in the experiment.

Close to the operation points for which $\partial I / \partial Q_g = 0$, the contribution from the quadratic term in eq. (3) becomes important. Assuming Gaussian noise we get

$$S_{I_Q}(f) \approx \left(\left(\frac{\partial I}{\partial Q_g} \right)^2 + \frac{\alpha}{4} \left(e \frac{\partial^2 I}{\partial Q_g^2} \right)^2 \right) S_{Q_g}(f) \quad (4)$$

where $\alpha(f) = [\int_{-\infty}^{+\infty} S_{Q_g}(f') S_{Q_g}(f - f') df'] / e^2 S_{Q_g}(f)$. For the SETs, we find $\alpha(f) \sim 10^{-4}$. This is smaller than the two orders of magnitude of dynamic range we have in the noise measurement and we can thus neglect the second term.

Now let us consider a different model in which Q_g does not fluctuate, and the only fluctuating parameter is the tunnel resistance R_1 of the first junction. (The fluctuations of the tunnel junction resistance have been extensively studied in large area junctions, see e.g., Refs. [22].) For simplicity let us limit ourselves to the linear term of the series expansion, so that $S_{IR_1}(f) = (\partial I / \partial R_1)^2 S_{R_1}(f)$, where $\partial I / \partial R_1$ can be calculated [4]. Note that S_{IR_1} is asymmetric around $Q_g = e/2$ as a function of Q_g for $V \leq \frac{e}{2C_\Sigma}$ [23], while it becomes independent of Q_g and proportional to V^2 for large V . Furthermore, the fluctuations of R_1 can in principle change with V , Q_g , and T (however, a strong dependence on V and Q_g is unlikely).

On the other hand the current noise which is due to Q_g fluctuations decreases for sufficiently large V because of the decrease in $|\partial I / \partial Q_g|$ and is symmetric around $Q_g = e/2$ for a symmetric SET-transistor. Therefore, the bias dependence and this asymmetry could be used to distinguish the charge fluctuations from the resistance fluctuations.

In general, the noise can also be caused by simultaneous fluctuations of Q_g , R_1 , and R_2 . If they are uncorrelated, the corresponding current spectral densities should simply add. However, fluctuators inside the tunnel barrier, which have been suggested as the source of the $1/f$ noise by several authors [8, 9, 15, 17], can be responsible for both resistance and charge fluctuations. Then, these contributions are correlated and we arrive at the following expression

$$\begin{aligned}
S_{I_{Q,R}}(f) &= \left(\frac{\partial I}{\partial Q_g}\right)^2 S_{Q_g}(f) + \left(\frac{\partial I}{\partial R_1}\right)^2 S_{R_1}(f) + \left(\frac{\partial I}{\partial R_2}\right)^2 S_{R_2}(f) \\
&+ K_1 \frac{\partial I}{\partial Q_g} \frac{\partial I}{\partial R_1} \sqrt{S_{Q_g}(f)S_{R_1}(f)} + K_2 \frac{\partial I}{\partial Q_g} \frac{\partial I}{\partial R_2} \sqrt{S_{Q_g}(f)S_{R_2}(f)} \quad (5)
\end{aligned}$$

K_i is the dimensionless correlation coefficient between Q_g and R_i fluctuations, $|K_i| \leq 1$.

The first term in eq. (5) describes the dominating gain dependent noise, while the other terms contribute to the excess noise. We can now compare the bias dependence of the excess noise measured in the Nb SET to that of eq. (5). From the integrated noise spectra we calculate the measured excess current noise $I_{n,exc}$, according to eq. (1) and plot it versus V in fig. 2b. $I_{n,exc}$ seems to increase with bias voltage, but there is no quadratic dependence which would be expected from eq. (5). It thus seems likely that the excess noise is *not* due to resistance fluctuations, but has a different origin. One possible explanation is that the increasing current heats the SET and generates more noise. Furthermore, at the highest bias point we can set an upper level for the resistance fluctuation in the frequency range from 51-99 Hz, δR_{51-99} . Assuming a symmetric SET ($R_1 = R_2$ and $S_{R_1} = S_{R_2}$) we get $\delta R_{51-99} < 31 \Omega_{RMS}$ for the Nb SET and $\delta R_{51-99} < 1.8 \Omega_{RMS}$ for the Al SET.

In conclusion we have measured the low frequency noise of two single electron transistors. In both transistors, the noise at the output closely followed the gain. This shows that low frequency noise in the SET is mainly due to external charge noise. When the gain was low, we observed an excess noise in the Nb SET for all bias voltages and in the Al SET for the highest bias voltage. From the bias dependence of the excess noise in the Nb SET we conclude that the main source of the excess noise is not resistance fluctuations. We also set an upper limit for the resistance fluctuations. The Al SET had a very high gain and showed a minimum charge noise $q_n \approx 2 \cdot 10^{-5} e/\sqrt{\text{Hz}}$ in both the superconducting and normal state, respectively.

4 Acknowledgements

We gratefully acknowledge discussions with K.K. Likharev and A.B. Zorin. The samples were fabricated in the Swedish Nanometer Laboratory. This work was sponsored by the Swedish SSF and NFR, by the ESPRIT project CHARGE and by the Japanese NEDO.

References

- [1] Likharev K. K., *IEEE Trans. Mag.* **23**, 1142 (1987)

- [2] Fulton T. A. and Dolan G. J., *Phys. Rev. Lett.* **59**, 109 (1987)
- [3] Schottky W., *Ann. Phys.* **57**, 541 (1918)
- [4] Korotkov A. N., Averin D. V., Likharev K. K. and Vasenko S. A. in *Single Electron Tunneling and Mesoscopic Devices*, edited by H. Koch (Springer, New York, 1992) p. 45
- [5] Birk H., de Jong M. J. M. and Schoenenberger C., *Phys. Rev. Lett.* **20**, 1610 (1995)
- [6] Kuzmin L. S., Delsing P., Claeson T. and Likharev K. K., *Phys. Rev. Lett.* **62**, 2539 (1989)
- [7] Zimmerli G., Eiles T. M., Kautz R. L. and Martinis J.M., *Appl. Phys. Lett.* **61**, 237 (1992)
- [8] Verbrugh S. M., Benhamadi M. L., Visscher E. H. and Mooij J. E., *J. Appl. Phys.* **78** (1995), 2830
- [9] Zorin A. B., Ahlers F.-J. , Niemeyer J., Weimann T., Wolf H., Krupenin V. A. and Lotkhov S. V., *Phys. Rev. B* **53**, 13682 (1996)
- [10] Starmark B., Delsing P., Haviland D. B. and Claeson T., in *Ext. Abstr. 6th International Superconductive Electronics Conference*, pp. 391-393, (Berlin, 1997)
- [11] Tavkhelidze A. N. and Mygind J., *J. Appl. Phys.* **83**, 310 (1998)
- [12] Bouchiat V., Ph.D. Thesis, Paris 6 (1997), pp. 202
- [13] Zimmerman N. M., Cobb J. L. and Clark A. F., *Phys. Rev. B* **56**, 7675 (1997)
- [14] Hergenrother J. M., Tuominen M. T., Tighe T. S. and Tinkham M., *IEEE Trans. Appl. Supercond.* **3**, 1980 (1993)
- [15] Song D., Amar A., Lobb C. J. and Wellstood F. C., *IEEE Trans. Appl. Supercond.* **5**, 3085 (1995)
- [16] Zorin A. B., Pashkin Y. A., Krupenin V. A. and Scherer H., in *Ext. Abstr. 6th International Superconductive Electronics Conference*, pp. 394-396, (Berlin, 1997)
- [17] Krupenin V. A., Presnov D. E., Scherer H., Zorin A. B. and Niemeyer J., cond-mat/9804197.
- [18] Niemeyer J. et. al., private communication
- [19] Machlup S., *J. Appl. Phys.* **25**, 341 (1954)

- [20] Dolan G. J., *Appl. Phys. Lett.* **31**, 337 (1977)
- [21] Zorin A. B., *Rev. Sci. Instrum.* **66**, 4296 (1995)
- [22] Rogers C. T. and Buhrman R. A., *Phys. Rev. Lett.* **53**, 1272 (1984); *Phys. Rev. Lett.* **55**, 859 (1985) Savo B., Wellstood F. C., and Clarke J., *Appl. Phys. Lett.* **50**, 1757 (1987).
- [23] The noise is larger when the current is determined by the fluctuating junction resistance to a greater extent than by the other junction.

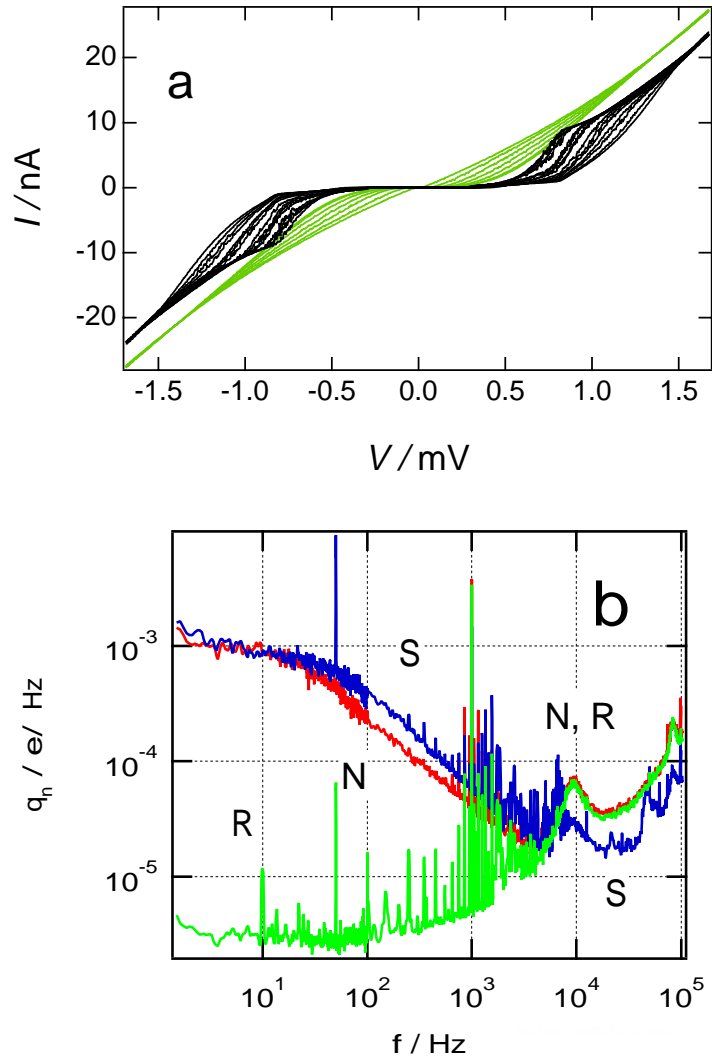


Figure 1: a) Current-voltage characteristics for the Al SET in the normal and superconducting state for several different gate charges. The curves were measured at $T = 30\text{mK}$. b) Noise spectra for the system for the normal (N) and superconducting (S) state and with no SET connected (R). The noise has been input referred to a charge noise (see text).

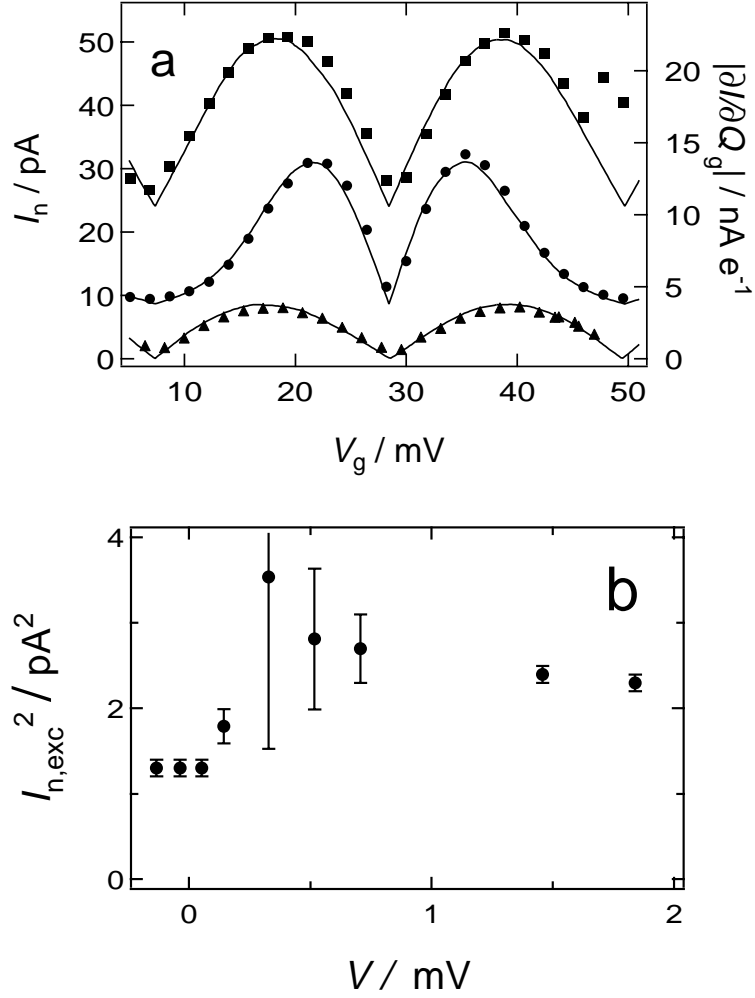


Figure 2: a) Gain (curves) and integrated output noise (symbols) vs gate bias for the Al SET. The bias voltage is $V = 0.25$ mV (middle curve), $V = 0.43$ mV (upper curve) and $V = 1.04$ mV (lower curve). The curves have been offset vertically for clarity. b) excess noise as a function of bias voltage for the Nb SET.

Appendix D

Appended Paper 3

Bias and temperature dependence of the noise in a single electron transistor

Torsten Henning, B. Starmark, T. Claeson, P. Delsing
Microelectronics and Nanoscience - Applied Solid State Physics
Göteborgs Universitet / Chalmers Tekniska Högskola AB
SE-41296 Göteborg, Sweden, Fax +46 31 772-3471

submitted to EPJ B: 1998-08-18
typo corrected 1998-08-20

PACS 73.23Hk Coulomb blockade; single-electron tunneling.
PACS 73.40Rw Metal-insulator-metal structures.

Abstract

A single electron transistor based on Al-AlO_x-Nb tunnel junctions was fabricated by shadow evaporation and in situ barrier formation. Its output current noise was measured, using a transimpedance amplifier setup, as a function of bias voltage, gain, and temperature, in the frequency range (1...300) Hz. The spot noise at 10 Hz is dominated by a gain dependent component, indicating that the main noise contribution comes from fluctuations at the input of the transistor. Deviations from ideal input charge noise behaviour are found in the form of a bias dependence of the differential charge equivalent noise, i. e. the derivative of current noise with respect to gain. The temperature dependence of this effect indicates that heating is activating the noise sources, and that they are located inside or in the near vicinity of the junctions.

1 Introduction

Single electron transistors with capacitive coupling ([C-]SET) [1, 2] are the most sensitive solid state electrometers available today [3]. They are limited in their accuracy by their noise, which increases with lower frequencies. The empirical relation between the spectral density $S_X(f)$ of the output quantity X (X being current I or voltage V depending on mode of operation, or input charge equivalent Q_g),

$$S_X(f) = S_X(f_0) \cdot \left(\frac{f}{f_0}\right)^{-\alpha}, \alpha \approx 1 \quad (1)$$

has lead to the nickname “ $1/f$ noise”. However, the deviation of α from unity is often significant. We will therefore use the more general term “low frequency noise”.

The low frequency noise has long since been assumed to be caused by charged particles oscillating randomly in traps, thus inducing a displacement charge on the island, and shifting the operating characteristics of the SET by fractions of an elementary charge. No conclusion has been reached as to the exact location of these traps, which are generally modelled as two level fluctuators. While some research groups expect them in the immediate (a few tenths of a nanometre) vicinity of the island, others have seen evidence that they might be at some distance [4, 5]. In the

latter case, they would have to be in the substrate, which is usually aluminium oxide or, as in our case, oxidised silicon on a silicon substrate.

A noise source in form of a charged particle trap inside the barrier between the island and the source/drain leads, on the other hand, might not only cause fluctuations of the island charge, but also of the barrier's resistance. Resistance fluctuations have been studied in larger junctions for a long time. Such a resistance fluctuation component of the noise in single electron transistors has been claimed to have been seen recently [6].

Previously, the noise of a system consisting of a SET, its electromagnetic environment, and the measurement setup was often described by referring the measured (output) noise to an input charge equivalent noise, by dividing voltage noise by the gate capacitance or current noise by the gain. The global minimum of this input referred noise over all bias and gate charge values at a certain frequency (it is customary to compare SET at 10 Hz) was then taken as a figure of merit, with a record low of $7 \cdot 10^{-5} e\text{Hz}^{-1/2}$ observed in a multilayer device [7].

In this paper, we present extensive measurements of the low frequency noise of a SET as a function of gate charge (or gain), bias (transport) voltage, and temperature, in order to investigate to what extent the noise has input noise character.

Niobium is an interesting material for single electronics, in comparison to aluminium prevailing to date, not only because of its higher critical temperature and energy gap, promising increased sensitivity of superconductive devices, but also because of the better stability against thermal cycling and ageing from which aluminium devices suffer. Therefore, even the operation of niobium based devices driven into the normal state, on which we will focus in this paper, is of practical interest.

2 Experimental details

2.1 Sample fabrication

Although some progress has been made in the introduction of niobium as a material for single electronics, some technological issues remain unsolved. So far, none of the available techniques can simultaneously fulfill all the three goals of

1. high energy gap Δ , as close as possible to the bulk value of 1.5 meV;
2. as high charging energy as possible; and
3. tunnel junction resistances higher than the quantum resistance 25.4 k Ω , but not too much higher than this value so as not to lose gain and, subsequently, output signal-to-noise ratio.

The conventional Niemeyer-Dolan (angular or shadow evaporation) technique [8, 9] that we used produces small junctions, and the barrier, which is formed in situ by oxidising the aluminium, can be tuned to reasonable resistance values below 100 k Ω per junction. The price for these advantages is a rather low value of Δ [10]. It cannot simply be explained by the low thickness of the electrodes, which are limited to a few tens of nanometres, since even such thin Nb films can have a Δ close to the bulk value if deposited under more ideal conditions [11].

The resist mask with its suspended bridges, however, prohibits the use of surface cleaning techniques like sputtering that have been found essential for the fabrication of high quality films [11]. In addition, outgassing of the organic resist components due to the intense heat of the niobium evaporation probably leads to inclusion of contaminants in the Nb film, and the critical temperature of niobium is very sensitive to contamination [12], especially by oxygen. A possible way out might be

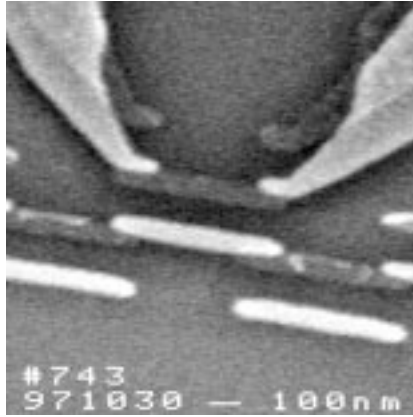


Figure 1: Scanning electron micrograph of a single electron transistor nominally identical to the sample under consideration, with Nb leads (bright) and an Al island. The excess island created by the double angle evaporation technique forms part of a linear array of junctions.

inorganic or more heat resistant organic resists that can be pre-baked at higher temperatures [13].

Other techniques have different drawbacks. The self-aligned in-line technique (SAIL) gives a high Δ and low junction capacitances, but rather high junction resistances and low gain [14]. A recently published modification [15] of the established three layer process using a prefabricated barrier in a sandwich structure gives a very good Δ , but it will have to be scaled down by about half an order of magnitude in linear dimensions before the charging energies reach those attainable by the Niemeyer-Dolan technique at present.

Our sample substrates of size $7 \times 7 \text{ mm}^2$ were made from silicon wafers thermally oxidised to a depth of $(900 \pm 100) \text{ nm}$. A gold pattern with contact leads and alignment fiducials was produced by photolithography. We used a four layer resist evaporation mask. It consisted of a bottom layer of 50 nm 950k PMMA baked at 170°C (to enable liftoff), a second layer of approximately 250 nm of Shipley S1813 photo resist baked at 160°C , providing support for the following layer of 20 nm germanium deposited by evaporation, and a top layer of 50 nm 950k PMMA. Electron beam lithograph patterning of the top layer was done with a JEOL JBX 5D-II system using a 20 pA beam at 50 kV, the “fifth” lens with a working distance of 14 mm, and the “first” aperture with a diameter of $60 \mu\text{m}$. The thinnest lines that were to form the SET were designed with a width of 20 nm, a centre-to-centre distance of 240 nm and an overlap of the parallel lines for leads and island of 100 nm. Proximity correction was done manually, and the thinnest structures, exposed at a dose of $1.7 \text{ mC}/\text{cm}^2$, had a final line width after processing of about 100 nm (see fig. 1).

After exposure and development for 60 s in a 10:1 (by volume) mixture of isopropanol and water under ultrasonic excitation, the pattern was transferred to the germanium layer by reactive ion etching (RIE) with carbon tetrafluoride CF_4 as the process gas at a pressure of 1.3 Pa, a flow rate of $7.5 \mu\text{mol}/\text{s}$, and an RF power of 14 W applied for 120 s (248 cm^2 electrode area, 60 mm electrode distance). The layers supporting the Ge mask were then etched by RIE in the same machine with O_2 as the process gas at a pressure of 13 Pa, a flow rate of $15 \mu\text{mol}/\text{s}$, and an RF power of 20 W applied for 15 min. These parameters gave an undercut profile sufficient for the subsequent angular evaporation.

Evaporation of both Al (purity 5N) and Nb (2N8) was carried out in a UHV system with a base pressure in the 10^{-7} Pa range, equipped with a load lock for the in situ oxidation of the barrier. First, the 20 nm thick Al bottom layer was deposited, at an angle of -21° to the substrate normal, by thermal evaporation from an effusion cell that delivered at a rate of only 3 nm/min. The resulting coarse grained structure of the Al film, with grain sizes of tens of nanometres, would have made it impossible to cover a Nb layer completely, as would be necessary for a Nb-AlO_x-Nb transistor. Thus, we chose Al as the base electrode material. It was oxidised in non-dehumidified air at a pressure of 8.8 Pa for 20 min, and after pumping down for 120 min, the Nb layer was deposited at an angle of $+21^\circ$ to the substrate normal. Unfortunately, we did not carry out any pre-evaporation of Nb against the closed shutter for this sample. Such a procedure might have improved the quality of the film [10]. The film was deposited by opening the shutter for 2 s and closing it for 8 s a total of five times. This practice was intended to reduce damage of the mask. Such a damage had been seen earlier, we had attributed it to overheating, but later found it to be caused by fabricating the resist incorrectly. The interval evaporation procedure was thus abandoned.

Two chips on a contiguous piece of substrate were processed simultaneously. One was taken for the measurements, while the second chip was subject to characterisation by scanning electron microscopy (SEM). Figure 1 shows the image of a transistor on the second chip corresponding to the one on the first chip on which the measurements described in the following were performed.

2.2 DC characterisation

The characterisation at very low temperatures as well as the noise measurements described in section 3 were carried out with the sample attached to the mixing chamber of an Oxford TLE 200 dilution refrigerator, reaching a base temperature of (30 ± 5) mK. All measurement leads were filtered by 500 mm of Thermocoax cabling [16]. The amplifier electronics were battery powered, and the data were read out with digital multimeters connected through shielded room feedthrough filters.

2.2.1 Normal conducting state

The sample's resistance, i. e. the combined resistance of both junctions $R_T = R_1 + R_2$, was measured between room temperature and 4.2 K one week after fabrication. It rose from (125 ± 5) k Ω at room temperature to (165 ± 8) k Ω at 4.2 K and high bias. The differential resistance around zero bias increased to about 215 k Ω due to the Coulomb blockade.

We did not find any significant change of R_T between this first characterisation and the subsequent characterisation and noise measurements at very low temperature, that were started one and three months after fabrication, respectively (all data presented here stem from the second set of measurements).

Figure 2 shows the current-voltage characteristics (IVC) of the sample at the dilution refrigerator's base temperature, when it was driven into the normal state by an external magnetic field of 5 T. The absence of a Coulomb staircase in the blockade indicates that the two junctions were fairly similar. Also, the spread in R_T values was less than 20 % among four nominally identical double junctions on the same chip.

The island capacitance C_Σ , i. e. the sum of the two junction capacitances $C_{1,2}$ and the capacitance to ground and gate C_0 (which is negligible), was determined by an offset voltage analysis [17] at base temperature. From an extrapolated zero bias offset voltage $V_{\text{off},0} = (325 \pm 15)$ μ V, we found $C_\Sigma = (0.49 \pm 0.02)$ fF.

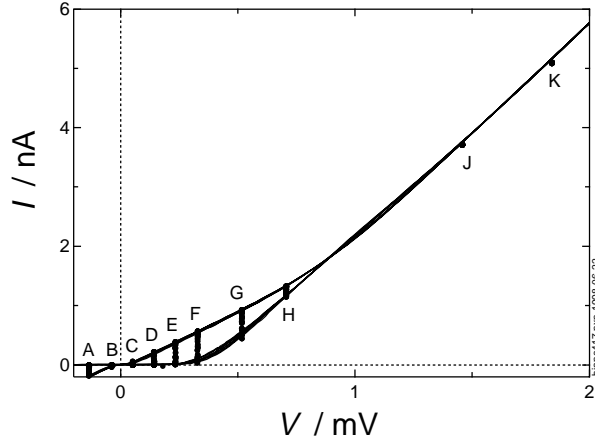


Figure 2: I - V characteristics of the single electron transistor at base temperature in the normal conducting state, with maximum and minimum blockade. The letters indicate the voltage bias points for the noise measurements.

The gate capacitance C_g was determined from the periodicity of the current-gate voltage characteristics, taken during the noise measurements, $V_p = e/C_g = (0.512 \pm 0.008)$ V, giving $C_g = (0.313 \pm 0.003)$ aF.

2.2.2 Superconducting case

We found a separation in voltage between the origin and the conductance peak at minimum Coulomb blockade in the differentiated current-voltage characteristics of (850 ± 20) μ V. Using $\Delta_{Al} = (190 \pm 10)$ μ eV, this means $\Delta_{Nb} = (235 \pm 15)$ μ eV, or a gap in the niobium leads (only) 25% higher than that of the aluminium island, corresponding to a critical temperature below 2 K. We believe that the niobium gap should be at least twice that of aluminium with our technique under optimised deposition conditions.

2.3 Noise measurement setup

We used a transimpedance amplifier, described in detail earlier [18], for the measurements of the low frequency noise. It is sketched in fig. 3. The sample was voltage biased symmetrically with respect to ground via two operational amplifiers with feedback resistors $R_B/2 = 10$ M Ω . The current signal was read out by a HP 35565 dynamic signal analyser that performed a real time Fast Fourier Transform of the signal. To increase resolution, the frequency range was divided into subranges; 25 spectra were averaged in a subrange ending at 100 Hz, and 100 spectra in the next subrange evaluated up to 300 Hz. Each measurement, for one combination of bias voltage and gate charge, took approximately five minutes.

At each bias point, 21 different gate voltages were applied, covering a range of about one and a half elementary charges induced on the gate. The bias points are shown superimposed on the current-voltage characteristics in fig. 2.

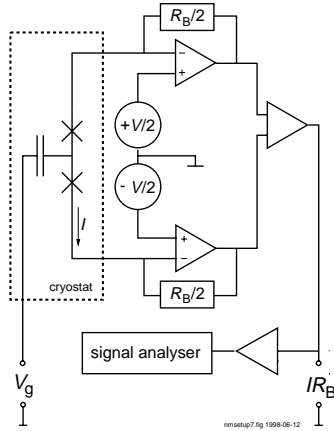


Figure 3: Transimpedance amplifier setup for current noise spectrum measurements. The sample is voltage biased symmetrically with respect to ground, and the amplified current signal is read out by a spectrum analyser.

3 Results

3.1 Noise spectral density

Over the frequency range between 1 Hz and 300 Hz, where we made our measurements, the amplifier noise

$$i_{n,\text{ampl}} = \sqrt{2k_B \frac{T_B}{R_B} + \frac{\epsilon_n^2(f)}{2r_0^2}} \quad (2)$$

(where ϵ_n is the input equivalent noise of the amplifier and $r_0 = dV/dI$ the output impedance of the SET) was almost entirely due to the thermal noise of the feedback resistors R_B , situated at room temperature T_B , so that we assumed $i_{n,\text{ampl}} = (28 \pm 2) \text{ fA}/\sqrt{\text{Hz}}$ over the whole range.

The transistor's gain dI/dQ_g was calculated from the gate capacitance $C_g = Q_g/V_g$ and the transconductance dI/dV_g , which in turn was calculated by numerically differentiating the current and gate voltage data taken simultaneously with the noise spectra. The sparseness in gate voltage points caused the uncertainty in our gain determination.

Attempts to measure the gain directly by superimposing a small ac component on the gate voltage and reading the corresponding ac component of the current with a lock-in technique were unsuccessful. Harmonics, subharmonics and beat frequencies, induced by crosstalk between input and output leads, blurred the noise spectrum if the ac amplitude was chosen sufficiently high to deliver a usable output signal, given our low gate capacitance.

Figure 4 shows the noise spectra in the points with the highest gains for both the normal and the superconducting states. Both spectra have been referred to the input by dividing with the respective gains, approximately $1.7 \text{ nA}/e$ in the normal and $3.4 \text{ nA}/e$ in the superconducting case. We see that the frequency dependence of the noise is the same in both the superconducting and the normal states, with an exponent of -0.8 in the charge noise (corresponding to $\alpha = 1.6$ in the power spectrum, eq. (1)). This behaviour, indicated by the dashed line in fig. 4, has also been found in all-aluminium SET on thermally oxidised silicon substrates [19].

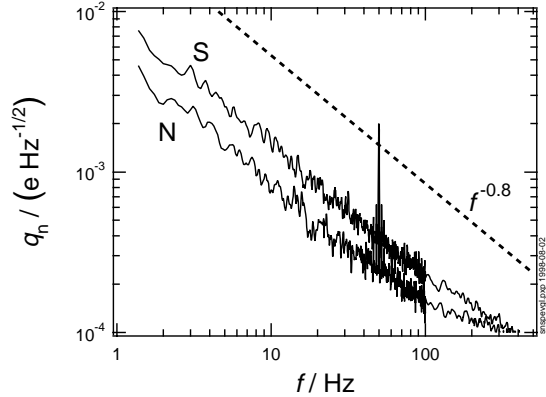


Figure 4: Charge equivalent noise spectra, at the bias and gate voltage points giving maximum gain, for the normal conducting (N, cf. fig. 2, point F) and superconducting (S) states, respectively. The dashed line indicates the frequency dependence $i_n \propto f^{-0.8}$.

The input charge equivalent noise in the superconducting state is almost equal to that in the normal state, which indicates the input character of the noise in this frequency range [19]. At the upper end of the frequency range, we see the crossover from input dominated to output dominated noise. Here, the input referred noise in the superconducting state falls significantly below that in the normal state, since the same output current noise in both states is divided by the higher gain in the superconducting state.

In the following, we will concentrate on the spot noise at the frequency 10 Hz, evaluated by a linear fit procedure in the bilogarithmic noise-frequency diagram. We will consider the net current noise, that is the measured current noise from which the (flat) amplifier noise and the shot noise contribution have been subtracted. Since the shot noise is only significant for the highest bias points well above the blockade (contributing with $40 \text{ fA}/\sqrt{\text{Hz}}$ at point K), we can neglect the suppression of the shot noise below and near the blockade and use the Poisson limit $i_{n,\text{Poi}} = \sqrt{2eI}$ [3].

3.2 Gain dependence of the current noise

It is immediately evident from fig. 5, showing net current noise and gain, respectively, plotted against gate charge for three bias points, that the noise follows the gain, or in other words, that the noise output can in first approximation be described as charge noise acting at the input of the SET [19]. For a more quantitative analysis, we plotted net current noise against gain for all bias points. An example for one bias point is shown in fig. 6.

The relation was always well described by a linear dependence, shown as a straight line in fig. 6. We will refer to the slope of the fit curve $q_n^{\text{fit}} = \langle di_n/d(dI/dQ_g) \rangle$, which has the dimension of a charge noise, as differential charge equivalent noise.

Any deviation from pure input noise behaviour should manifest itself in a systematic deviation from the linear relation. As we see from the inset in fig. 6, the fit residuals are spread fairly randomly, so within our measurement accuracy, we cannot identify another noise component with gain dependence, like the correlation between resistance noise and charge noise. For this correlation noise, the square of the current noise, $S_I = i_n^2$, should depend linearly on the gain [19].

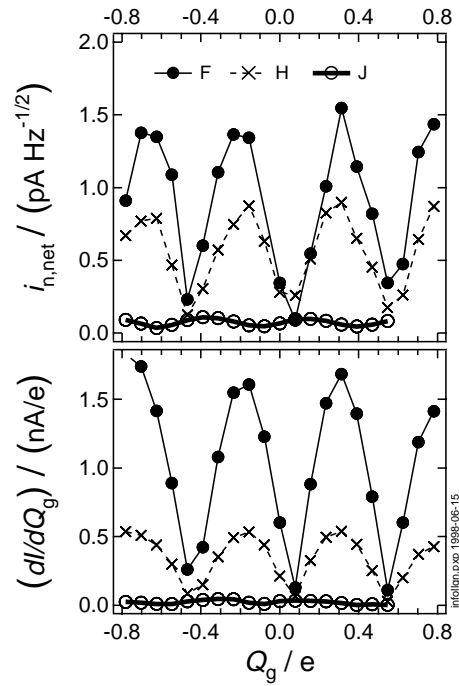


Figure 5: Change of the net current noise at 10 Hz (top panel; amplifier noise and shot noise have been subtracted) and of the gain (bottom panel) with the charge induced on the gate of the SET. Bias points are labelled as in fig. 2. Base temperature, normal state.

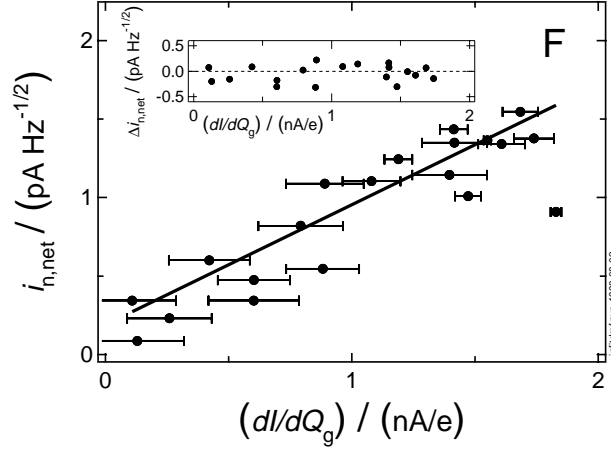


Figure 6: Dependence of the net current noise at 10 Hz on the gain. The thick line shows is a linear least squares fit to the data points, whose residuals are shown in the inset. The error margin on the gain is relatively large due to the small number of gate voltage points per bias point. Base temperature, normal state, bias point F.

The second order input charge noise contribution can generally be described [19] by the coefficient α in the expansion

$$S_{I_Q}(f) \approx \left(\left(\frac{\partial I}{\partial Q_g} \right)^2 + \frac{\alpha}{4} \left(e \frac{\partial^2 I}{\partial Q_g^2} \right)^2 \right) S_{Q_g}(f), \quad (3)$$

where $S_{I_Q}(f)$ is the output noise generated by the input charge noise $S_{Q_g}(f)$, and α can be evaluated as

$$\alpha(f) = \frac{1}{e^2 S_{Q_g}(f)} \int_{-\infty}^{+\infty} S_{Q_g}(f') S_{Q_g}(f - f') df'. \quad (4)$$

We found that $\alpha \approx 10^{-4}$, practically independent of frequency. Second order contributions from this term can thus be neglected within our measurement accuracy.

3.3 Deviations from ideal charge noise behaviour

We will now inspect closer the gain dependent noise component to see if it behaves as we would expect for a pure input charge noise.

3.3.1 Bias dependence

In fig. 7, the linear fit of current noise versus gain relation from fig. 6 is shown for the five bias points around the global gain maximum. Comparing with the nomenclature of fig. 2, it is obvious that the slope of the fit curves, the differential charge equivalent noise, increases with the bias voltage.

In the simple model of low frequency noise in SET [19], we would expect such a dependence only as a second order effect, via a bias dependence of the input charge noise itself. The observed bias dependence indicates that the noise sources must be located quite close to the current path, since it seems implausible that distant defects should be affected by the small transport voltages or currents. The

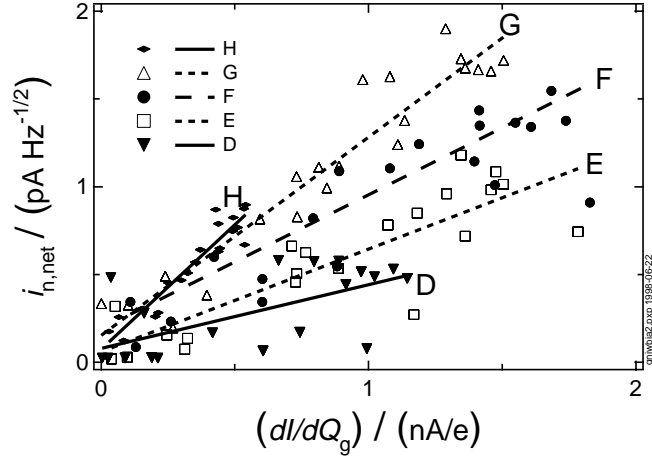


Figure 7: Gain dependence of the net current noise (amplifier noise and shot noise have been subtracted) at 10 Hz (base temperature, normal state). With increasing bias (D...H, cf. fig 2), the ratio between noise and gain increases, from $0.36 \times 10^{-3} e/\sqrt{\text{Hz}}$ at bias point D to $1.42 \times 10^{-3} e/\sqrt{\text{Hz}}$ at point H. These slopes have been determined by a least square fit to the data as illustrated in fig. 6, error bars and residuals have been omitted to reduce clutter.

immediate practical implication of the bias dependence of the output noise is that for low noise operation, a SET should be operated in the low bias region, where of course a tradeoff against signal amplitude will have to be made.

3.3.2 Temperature dependence

A possible mechanism, via which the bias could influence the noise sources, is heating of the barriers, the island, and the leads and surfaces in their vicinity, by the dissipation near the junctions. This was suggested as an explanation of the observed weak current dependence ($\propto I^{1/4}$) of the low frequency noise [20]. Measurements of the temperature dependent behaviour of a single two level fluctuator [21] corroborate this explanation, if one agrees with the common assumption that the low frequency noise is the effect of a large number of uncorrelated such two level fluctuators.

The measurements at base temperature, described above, were repeated at temperatures of 350 mK and 670 mK to test the heating hypothesis. Figure 8 shows the differential charge equivalent noise, calculated by the procedure demonstrated in figs. 6 and 7, plotted against bias voltage for the three temperatures. The error margin has been estimated from the average amplitude of the fit residual.

For base temperature, we see the clear increase of the differential charge equivalent noise with bias voltage that we found earlier. With increasing temperature, the zero bias value becomes significantly different from zero, and at a temperature of the order of half a Kelvin, the bias voltage dependence has vanished.

At the highest bias points (J and K), the differential charge equivalent noise was masked completely by zero gain noise and could not be determined.

This temperature dependence partly lifts the above stated possibility of minimising the noise by operating the SET at low bias. At higher temperatures, the input noise becomes independent of the bias, and therefore one can only minimise

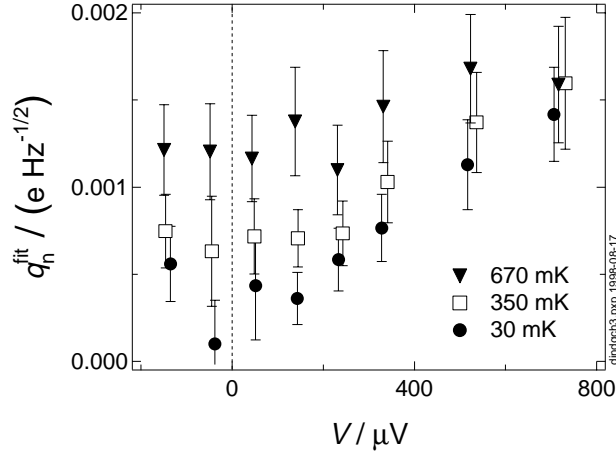


Figure 8: Differential charge equivalent noise (proportionality constant relating gain increase to current noise increase), as a function of bias voltage and at different temperatures. The values were determined as the slopes of the linear fit curves in the noise current versus gain diagrams (cf. fig. 6). The error margins were estimated from the average amplitude of the fit residuals.

the noise in the SET by maximising the gain.

3.3.3 Zero gain noise

Another deviation from the ideal input charge noise behaviour is the gain independent component that we call “zero gain noise” or “excess noise” [19]. It can simply be determined as the offset along the noise axis in the fit procedure used for calculating the differential charge equivalent noise.

Figure 9 shows the zero gain noise as a function of bias. The dependence is essentially the same as that of the excess noise calculated earlier as an integral in the frequency band between 50 and 100 Hz [19]. In any case, the zero gain noise has a peak around the bias point where the current modulation is maximal, and is practically independent of temperature. At the present time, we have no conclusive interpretation of the cause of this excess noise.

4 Conclusions

In studying the low frequency noise of a single electron transistor, we found that the output current noise is dominated by a component proportional to the gain of the transistor, which can be described as input charge noise. We found that the noise level of the transistor, expressed as the coefficient relating output noise to gain, increases with the bias voltage. At low temperature, low bias conditions are preferable for low noise operation of the SET. The bias dependence of the noise clearly indicates that the current through the SET is activating the background charges. This can be interpreted as a heating effect, corroborating the general belief that the charge noise sources are situated inside or in the near vicinity of the tunnel junctions. At higher temperature, the bias dependence of the noise disappears, and the transistor should be operated at maximum gain for optimal noise properties.

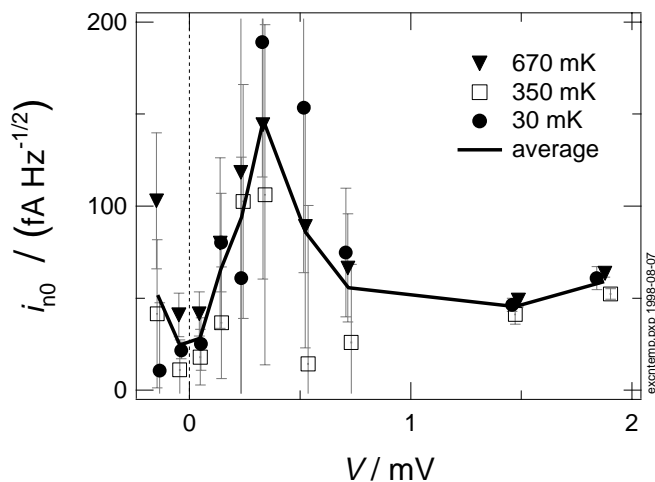


Figure 9: Zero gain noise at 10 Hz (normal conducting state) as a function of bias voltage, for the same temperatures as in fig. 8. The values were calculated from the vertical axis intersection in the fit procedure illustrated in fig. 6, the errors have been estimated from the ratio between the average amplitude of the fit residuals and the gain range.

Acknowledgements

Discussions with A. N. Korotkov on modelling the low frequency noise in SET are gratefully acknowledged. Our samples were made using the Swedish Nanometre Laboratory, Göteborg. This work is part of the ESPRIT project 22953 CHARGE, and we were supported by Stiftelsen för Strategisk Forskning as well as the Swedish agencies NFR and TFR.

References

- [1] Hermann Grabert and Michel H. Devoret, editors. *Single Charge Tunneling. Coulomb Blockade Phenomena in Nanostructures*, volume 294 of *NATO ASI Series*. Plenum Press, New York, 1992. ISBN 0-306-44229-9.
- [2] Alexander N. Korotkov. Coulomb blockade and digital single-electron devices. *cond-mat/9602165*, February 1996.
- [3] A. N. Korotkov, D. V. Averin, K. K. Likharev, and S. A. Vasenko. Single-electron transistors as ultrasensitive electrometers. In H. Koch and H. Lübbig, editors, *Single-Electron Tunneling and Mesoscopic Devices*, number 31 in *Springer Series in Electronics and Photonics*, pages 45–59. Springer, Berlin, 1992. Proceedings of the 4th International Conference SQUID '91.
- [4] A. B. Zorin, F.-J. Ahlers, J. Niemeyer, T. Weimann, H. Wolf, V. A. Krupenin, and S. V. Lotkhov. Background charge noise in metallic single-electron tunneling devices. *Phys. Rev. B*, 53(20):13682–13687, May 1996.
- [5] Neil M. Zimmerman, Jonathan L. Cobb, and Alan F. Clark. Modulation of the charge of a single-electron transistor by distant defects. *Phys. Rev. B*, 56(12):7675–7678, September 1997.

- [6] V. A. Krupenin, D. E. Presnov, M. N. Sarateev, H. Scherer, A. B. Zorin, and J. Niemeyer. Noise in Al single electron transistors of stacked design. *cond-mat/9804197*, April 1998.
- [7] E. H. Visscher, S. M. Verbrugh, J. Lindeman, P. Hadley, and J. E. Mooij. Fabrication of multilayer single-electron tunneling devices. *Appl. Phys. Lett.*, 66(3):305–307, January 1995.
- [8] Jürgen Niemeyer. Eine einfache Methode zur Herstellung kleinster Josephson-Kontakte. *PTB-Mitt.*, 84(4):251–253, 1974.
- [9] G. J. Dolan. Offset masks for lift-off photoprocessing. *Appl. Phys. Lett.*, 31(5):337–339, September 1977.
- [10] Y. Harada, D. B. Haviland, P. Delsing, C. D. Chen, and T. Claeson. Fabrication and measurement of a Nb based superconducting single electron transistor. *Appl. Phys. Lett.*, 65(5):636–638, August 1994.
- [11] Sung I. Park and T. H. Geballe. Superconducting tunneling in ultrathin Nb films. *Phys. Rev. Lett.*, 57(7):901–904, August 1986.
- [12] N. Elyashar and D. D. Koelling. Self-consistent relativistic APW calculation of the electronic structure of niobium with a non-muffin-tin potential. *Phys. Rev. B*, 15(8):3620–3632, April 1977.
- [13] A. K. Jain, J. E. Sauvageau, D. B. Schwartz, K. T. Springer, and J. E. Lukens. Fabrication of niobium-lead tunnel junctions using a self aligned masking technique. *IEEE Trans. Magnetics*, MAG-21(2):955–958, March 1985.
- [14] Klaus Blüthner, Martin Götz, Andreas Hädicke, Wolfram Krech, Thomas Wagner, Holger Mühlig, Hans-Jörg Fuchs, Uwe Hübner, Detlef Schelle, Ernst-Bernhard Kley, and Ludwig Fritzsche. Single-electron transistors based on Al/AlO_x/Al and Nb/AlO_x/Nb tunnel junctions. *IEEE Trans. Appl. Supercond.*, 7(2):3099–3102, June 1997.
- [15] Alexey B. Pavolotsky, Thomas Weimann, Hansjörg Scherer, Vladimir A. Krupenin, Jürgen Niemeyer, and Alexander B. Zorin. Multilayer technique developed for fabricating Nb-based single-electron devices. *cond-mat/9804192*, April 1998.
- [16] A. B. Zorin. The thermocoax cable as the microwave frequency filter for single electron circuits. *Rev. Sci. Instrum.*, 66(8):4296–4300, August 1995.
- [17] P. Wahlgren, P. Delsing, and D. B. Haviland. Crossover from global to local rule for the Coulomb blockade in small tunnel junctions. *Phys. Rev. B*, 52(4):R2293–R2296, July 1995.
- [18] B. Starmark, P. Delsing, D. B. Haviland, and T. Claeson. Noise measurements of single electron transistors using a transimpedance amplifier. In H. Koch and S. Knappe, editors, *ISEC'97. 6th International Superconductive Electronics Conference. Extended Abstracts*, volume 2, pages 391–393, Berlin, June 1997. Physikalisch-Technische Bundesanstalt. ISBN 3-9805741-0-5.
- [19] B. Starmark, T. Henning, A. N. Korotkov, T. Claeson, and P. Delsing. Gain dependence of the noise in the single electron transistor. *cond-mat/9806354*.

- [20] Henning Wolf, Franz Josef Ahlers, J. Niemeyer, Hansjorg Scherer, Thomas Weimann, Alexander B. Zorin, Vladimir A. Krupenin, Sergey V. Lotkhov, and Denis E. Presnov. Investigation of the offset charge noise in single electron tunneling devices. *IEEE Trans. Instrumentation and Measurement*, 46(2):303–306, April 1997.
- [21] M. Kenyon, A. Amar, D. Song, C. J. Lobb, F. C. Wellstood, Jonathan L. Cobb, and Neil M. Zimmerman. Dynamics of a charged fluctuator in an Al-AlO_x-Al single-electron transistor. unpublished, 1998.